Hydrol. Earth Syst. Sci. Discuss., 12, 12649–12701, 2015
www.hydrol-earth-syst-sci-discuss.net/12/12649/2015/
doi:10.5194/hessd-12-12649-2015

Hydrology and Earth System Sciences
Open Access
Discussions

Hierarchy of climate and hydrological uncertainties in transient low flow projections

J.-P. Vidal[1], B. Hingray[2,3], C. Magand[4,5], E. Sauquet[1], and A. Ducharne[4]

[1]Irstea, UR HHLY, Hydrology-Hydraulics Research Unit, Villeurbanne, 69100, France
[2]CNRS, LTHE UMR 5564, Grenoble, 38000, France
[3]Université Grenoble Alpes, LTHE UMR 5564, Grenoble, 38000, France
[4]Sorbonne Universités, UPMC, CNRS, EPHE, UMR 7619 METIS, 4 place Jussieu, 75005 Paris, France
[5]IPSL, LSCE, UPMC, CNRS, UVSQ, 4 place Jussieu, 75005 Paris, France

Received: 30 October 2015 – Accepted: 3 November 2015 – Published: 4 December 2015

Correspondence to: J.-P. Vidal (jean-philippe.vidal@irstea.fr)

Published by Copernicus Publications on behalf of the European Geosciences Union.

Abstract

This paper proposes a methodology for estimating the transient probability distribution of yearly hydrological variables conditional to an ensemble of projections built from multiple general circulation models (GCMs), multiple statistical downscaling methods (SDMs) and multiple hydrological models (HMs). The methodology is based on the quasi-ergodic analysis of variance (QE-ANOVA) framework that allows quantifying the contributions of the different sources of total uncertainty, by critically taking account of large-scale internal variability stemming from the transient evolution of multiple GCM runs, and of small-scale internal variability derived from multiple realizations of stochastic SDMs. The QE-ANOVA framework was initially developed for long-term climate averages and is here extended jointly to (1) yearly anomalies and (2) low flow variables. It is applied to better understand possible transient futures of both winter and summer low flows for two snow-influenced catchments in the southern French Alps. The analysis takes advantage of a very large dataset of transient hydrological projections that combines in a comprehensive way 11 runs from 4 different GCMs, 3 SDMs with 10 stochastic realizations each, as well as 6 diverse HMs. The change signal is a decrease in yearly low flows of around −20 % in 2065, except for the most elevated catchment in winter where low flows barely decrease. This signal is largely masked by both large- and small-scale internal variability, even in 2065. The time of emergence of the change signal on 30 year low-flow averages is however around 2035, i.e. for time slices starting in 2020. The most striking result is that a large part of the total uncertainty – and a higher one than that due to the GCMs – stems from the difference in HM responses. An analysis of the origin of this substantial divergence in HM responses for both catchments and in both seasons suggests that both evapotranspiration and snowpack components of HMs should be carefully checked for their robustness in a changed climate in order to provide reliable outputs for informing water resource adaptation strategies.

HESSD

12, 12649–12701, 2015

1 Introduction

Incorporating global change in long-term water resource planning, water management and water governance is a major issue water managers currently have to face (see e.g. Clarvis et al., 2014; Bréthaut and Hill Clarvis, 2015). Indeed, hydrological impacts of climate change may significantly alter amounts and timing of both the water demand and the water availability. Future water availability informing water resource adaptation strategies are usually assessed based on hydrological modelling with forcings from General Circulation Model (GCM) projections for specific catchments and/or at the national scale (see e.g. Christierson et al., 2012; Chauveau et al., 2013). In this context, a water manager with some degree of awareness in potential climate change impact studies is entitled to ask the following question, particularly relevant for long-term planning: for a given year in the future, what will be the probability of having a low flow value lower than a given baseline? Note that a very similar question has been recently addressed by Sexton and Harris (2015) on the probability of a seasonal temperature/precipitation average for a given year being lower or higher than a present-day baseline. In order to answer the water manager question, one should address four different scientific issues: (1) computing future hydrological changes, (2) generating a transient evolution of those changes, (3) disentangling hydrological change signal from effects of natural/internal climate variability, and (4) focusing on the lower part of the streamflow distribution. The following paragraphs proposes a brief review of how such issues listed above have been tackled in the literature.

The first issue has been largely addressed in the literature over the last decades, through the use of hydrometerological modelling chains composed of GCMs, downscaling techniques – either regional climate models or statistical downscaling techniques (SDMs) – and hydrological models (HMs). Such hydrometerological chains provide a quantification of the hydrological change signal, but also an estimate of the uncertainty associated to each level of the modelling chain, provided of course that they include multiple models at each level (Wilby and Dessai, 2010). There is

HESSD
12, 12649–12701, 2015

a growing body of literature on the quantification of the contribution of each level of the hydrometeorological chain to the overall modelling uncertainty in hydrological changes (Dobler et al., 2012; Finger et al., 2012; Bosshard et al., 2013; Hagemann et al., 2013; Addor et al., 2014; Lafaysse et al., 2014; Schewe et al., 2014; Giuntoli et al., 2015; Vetter et al., 2015). In most cases, contributions from the different sources of uncertainty are derived through more or less formal analysis of variance (ANOVA) techniques which recently became a common tool in climate studies (Yip et al., 2011; Sansom et al., 2013).

These projections are however historically and still generally derived for specific time slices in the future, and only few studies engaged in deriving transient hydrological projections (Lafaysse et al., 2014; Barria et al., 2015).

The issue of quantifying internal climate variability and its additional contribution to modelling uncertainty has retained much attention from the climate community over the last few years (Hawkins and Sutton, 2009, 2011; Deser et al., 2012). The quantification of global climate variability has been recently propagated downstream the modelling cascade in some hydrological studies (Lafaysse et al., 2014; Seiller and Anctil, 2014; Gelfan et al., 2015; Peel et al., 2015; van Pelt et al., 2015). When internal variability is estimated from the analysis of multiple runs from a GCM in most studies, alternatives have been proposed to circumvent the often low number of available runs which prevent simple robust estimations (see e.g. Peel et al., 2015). Another type of internal variability has moreover been taken into account in a few regional studies: the variability of small-scale meteorological features given a signal from GCMs, estimated from stochastic downscaling methods (either perfect-prog methods or weather generators) (Lafaysse et al., 2014; Fatichi et al., 2015; Peel et al., 2015).

Lastly, the first objective of the majority of hydrological changes studies so far was on streamflow regime. When some of them explored changes in the entire flow duration curve (Dobler et al., 2012; Bosshard et al., 2013; Fatichi et al., 2015), relatively few focused on the lower end of the hydrological spectrum (see e.g. Wilby and Harris, 2006; Giuntoli et al., 2015; Vetter et al., 2015).

HESSD
12, 12649–12701, 2015

The objective of this work is to deliver relevant information on possible futures of low flows for informing water resource adaptation strategies. To this aim, it attempts to answer the water manager question by addressing all four issues listed above for two specific snow-influenced Alpine catchments with high stakes on water resources. This work takes advantage of a very large dataset of transient 1980–2065 hydrological projections that combines in a comprehensive way 11 runs from 4 different GCMs, 3 SDMs with 10 stochastic realizations each, as well as 6 diverse HMs. Time series of mean annual minimum flow over 7 days are first derived separately for winter and summer for both catchments and for each of the 1980 hydrological projections. The quasi-ergodic analysis of variance (QE-ANOVA) framework developed by Hingray and Saïd (2014) is applied on this low flow dataset to quantify the relative contributions of model uncertainty due to GCMs, SDMs and HMs, but also critically of both large-scale and local-scale components of internal variability. This framework is here extended to analyse not only changes in time-slice averages, but also yearly anomalies, in order to take account of the year-to-year variability that is of much interest for operational water management.

Section 2 introduces the two case study catchments and describes the hydrological projection dataset used. Section 3 presents the selected low flow indicator for two separate seasons and details the QE-ANOVA approach and its adaptation and extension to yearly anomalies of low flows. Results are given in Sect. 4 and discussed in Sect. 5.

2 Data

2.1 Case study catchments

The Durance basin is located in the Southern French Alps, and water flows into the Rhône river. This basin has a total area of 14 000 km^2 and an altitude range of 4000 m. It carries high stakes for water resources as it produces 10 % of French hydropower

HESSD
12, 12649–12701, 2015

and supplies drinking water to approximately 3 million people (Warner, 2013). It is moreover exposed to various climatic influences, from Alpine climate in the upper northern part to Mediterranean climate in the lower southern part. Water resources are already under high pressure due to substantial abstractions within and out of the river basin, and global change will question the sustainability of the current rules for water allocation among the different uses, among all other governance challenges (Bréthaut and Hill Clarvis, 2015). The R2D2-2050 project addressed this issue by building projections of future water availability, prospective scenarios of water demand, as well as prospective scenarios of future water management (Sauquet et al., 2014).

Two case study catchments are considered here: the Durance@Serre-Ponçon and the Verdon@Sainte-Croix (see Fig. 1). They have been selected here for two main reasons: first, they are located upstream the two largest reservoirs in the Durance catchment, the Serre-Ponçon reservoir being actually the second largest in Europe. The management of these reservoirs is coordinated to fulfil water demands from various uses. Second, their hydrological regime is largely influenced by snowpack/snowmelt processes, with differences stemming from their altitude range and geographical location. The Durance@Serre-Ponçon (3580 km^2) is located in the heart of the French Alps and more than half of its area is above 2500 m, whereas the Verdon@Sainte-Croix (1620 km^2) is located on the southern Mediterranean edge of the Alpine range, with a maximum altitude of 2500 m.

Reconstitutions of natural streamflow for both stations were provided by the EDF power company which manages both Serre-Ponçon and Sainte-Croix reservoirs. Reconstructed streamflow were derived prior to the R2D2-2050 project from outflows and stored volumes in the two reservoirs, and corrected from the influence of other upstream hydropower reservoir operations.

HESSD
12, 12649–12701, 2015

2.2 Hydrological projection dataset

2.2.1 Global climate projections

Climate projections over the Durance basin are based on global projections from the ENSEMBLES project (van der Linden and Mitchell, 2009), and more specifically from the STREAM2 simulations using more recent versions of the GCMs (Johns et al., 2011). The simulations used here are forced by 20C3M forcings (historical forcing by greenhouse gases and aerosols) until year 2000, and emissions from the A1B scenario afterwards (Nakićenović et al., 2000). Table 1 lists the GCM runs for which appropriate variables for downscaling were available and that were used in this study. The specific period considered here runs from 1 August 1958 to 31 July 2065.

2.2.2 Downscaled climate projections

The spatial resolution of the global projections is not adapted to hydrological modelling over small areas like the Durance basin. A downscaling step has therefore been performed within a previous project on this basin (RIWER2030, Hingray et al., 2013). Three statistical downscaling methods (SDMs) have been applied here, all of them primarily based on the analogue principle introduced by Lorenz (1969). This principle is based on the assumption that similar large-scale atmospheric circulation patterns lead to similar local-scale values of near-surface meteorological variables. SDMs build statistical relationships between an archive for predictors and an archive for predictands. For each GCM run, each SDM provides 100 stochastic realizations of meteorological time series in order to generate a probabilistic output of the downscaling step (see Lafaysse et al., 2014, for details on the stochastic generation process). All three methods have been extensively used in previous climate change impact studies (see e.g. Bourqui et al., 2011; Vidal et al., 2012; Chauveau et al., 2013; Lafaysse et al., 2014), and their main characteristics are given in Table 2. Further details on the SDMs are given by Hingray and Saïd (2014) and Lafaysse et al. (2014).

HESSD
12, 12649–12701, 2015

The archive for predictor is the NCEP/NCAR global reanalysis (Kalnay et al., 1996) and the archive for predictands is the DuO near-surface reanalysis (Magand et al., 2014) built as a hybrid between the SPAZM (Gottardi et al., 2012) and Safran (Vidal et al., 2010) reanalyses. DuO combines the higher spatial resolution of SPAZM ($1\,km^2$) – relevant for example for high-altitude precipitation – and the higher temporal resolution (hourly) and the additional variables (including wind and radiation) of Safran that are required inputs for land surface models. The period considered as an archive for analogue dates runs from 1 August 1980 to 31 July 2005 (Hingray et al., 2013). Local-scale variables for target dates are taken as the ones from each analogue date. The Penman–Monteith reference evapotranspiration (ET0, Allen et al., 1998) required as an input by conceptual models is additionally computed from meteorological variables. An additional correction on the temperature of the analogue date is moreover potentially applied to ensure the consistency with large-scale regional temperature from the GCM (Mezghani and Hingray, 2009; Boé et al., 2009; Hingray et al., 2013). When such a correction is applied, related meteorological variables like infrared radiation or specific humidity from the analogue date are also corrected for ensuring inter-variable consistency following Etchevers et al. (2002).

The downscaling process thus led to 3300 (11 GCM runs × 3 SDMs × 100 realizations) hourly/daily gridded climate projections over the Durance catchment for the period 1 August 1958 to 31 July 2065. A subsampling of 10 realizations out of 100 from each combination of SDM and GCM run has next been applied to reduce the number of different forcings for the impact models and therefore lighten the computational burden by an order of magnitude. This subsampling was made through a Latin Hypercube Sampling (LHS) approach, which allows to subsample a multidimensional distribution while preserving its marginal properties (McKay et al., 1979; Minasny and McBratney, 2006). This approach has been recently used by Christierson et al. (2012) and Green and Weatherhead (2014) to sample the UKCP09 probabilistic climate projections (Murphy et al., 2009).

HESSD
12, 12649–12701, 2015

2.2.3 Hydrological projections

Six hydrological models have been run by different R2D2-2050 project partners over up to 26 catchments in the Durance basin during the project. Only simulations with GCM-driven forcings described above at the two selected catchments described in Sect. 2.1 are considered In the present work. The main characteristics of the 6 models are shown in Table 3. Most of them have been extensively used in previous climate change impact and adaptation studies in other French catchments, often in multimodel contexts (see e.g. Paiva et al., 2010; Moatar et al., 2010; Bourqui et al., 2011; Chauveau et al., 2013; Habets et al., 2013). Hydrological models have been calibrated against naturalized streamflow data over the reference period 1980–2009 – called REF in the following – except for ORCHIDEE for which default parameters were used. It has to be noted that CLSM and ORCHIDEE are land surface models initially built for running in a coupled mode with GCMs.

The hydrological modelling step thus led to 1980 daily streamflow time series from 1980 to 2009 for each of the two catchment case studies.

3 Methods

3.1 Low flow indicator

The low flow indicator chosen here is the Mean Annual Minimum flow over 7 days (MAM7) (WMO, 2008). In Alpine catchments influenced by snowpack/snowmelt processes, two distinct low flow periods can be identified with different underlying physical processes (see, e.g. Laaha and Blöschl, 2006a, b; Laaha et al., 2013). Summer low flows occur as a consequence of persistent dry and warm weather periods when evaporation exceeds precipitation. Winter low flows occur when precipitation is temporarily stored in the snow cover causing runoff recession. Two distinct seasons are therefore considered for computing the MAM7: summer (1 June–31 October) and

HESSD
12, 12649–12701, 2015

winter (1 November–31 May). Figure 2 shows these two low flow seasons and the observed daily interannual regime over the REF period for the two catchment case studies. Low flow seasons are less well marked for the low elevation Verdon@Sainte-Croix which experiences a higher interannual variability of autumn flows due to potentially heavy rainfall events.

3.2 The Quasi-Ergodic ANOVA framework

3.2.1 General principles

The partitioning of uncertainties in hydrological projections is performed in the framework of the quasi-ergodic analysis of variance (QE-ANOVA) framework developed by Hingray and Saïd (2014). This framework allows disentangling model uncertainty from internal variability in any unbalanced multimember multimodel ensemble, as the one available here. Model uncertainty components are estimated from the noise-free change signals (NFSs) of the different modeling chains using a classic analysis of variance framework. Internal climate variability components are then estimated based on the residuals from the NFSs, relying on the quasi-ergodic assumption for transient climate simulations. The paragraph below describes briefly the QE-ANOVA framework and the reader is referred to Hingray and Saïd (2014) for more details on the methodology, and to Lafaysse et al. (2014) for an application to hydrological variables.

Previous applications of the QE-ANOVA framework focused on changes in time-slice averages of the raw data y. In the following equations, the variable studied is noted Y and represents such a time-slice average. Equation (2) defines the relative change of the variable studied Y with respect to a baseline Y_0, for any prediction lead time t:

$$\Delta(g,s,h,r,k,t) = \frac{Y(g,s,h,r,k,t)}{Y_0} - 1 \quad (1)$$

HESSD
12, 12649–12701, 2015

where g, s and h are indices over GCMs, SDMs and HMs, respectively, r is an index over runs from a given GCM, and k an index of stochastic realizations from a given SDM. In the following, m will denote a GCM-SDM-HM modelling chain as a short for (g,s,h). The relative change Δ may be written as:

$$\Delta(m,r,k,t) = \mathrm{NFS}(m,t) + \eta(m,r,k,t) \quad (2)$$

where $\mathrm{NFS}(m,t)$ is the noise-free signal of the change variable for chain m, i.e. the estimated response of the modelling chain, and $\eta(m,r,k,t)$ are the residuals of stochastic realization k of SDM s for the run r of GCM g. The total uncertainty of Δ corresponds to the sum of variances of both terms on the right hand side of Eq. (2). They correspond respectively to the model uncertainty and to the internal variability of Δ for the modelling chains. Their different components are estimated as follows.

3.2.2 Deriving noise-free change signals (NFSs)

NFSs are estimated by first fitting trend models to the raw data y for each of the modelling chains, considering all available GCM runs and all SDM stochastic realizations available for this specific chain. NFSs are then obtained by considering relative changes of these trend models with respect to the baseline Y_0:

$$\mathrm{NFS}(m,t) = \frac{\hat{y}(m,t)}{Y_0} - 1 \quad (3)$$

where $\hat{y}$ is the trend model output. In the present work, Y_0 is taken as the average of the trend model over the reference period for a given modelling chain:

$$Y_0(m) = \overline{\hat{y}(m,t)|_{t\in \mathrm{REF}}} \quad (4)$$

This choice has also been made by Bracegirdle et al. (2014) and is similar to the approach of Charlton-Perez et al. (2010) who considered changes with respect to a fitted trend value for a given reference year.

HESSD
12, 12649–12701, 2015

3.2.3 Partitioning model uncertainty

NFSs can be partitioned into GCM, SDM and HM contributions through a 3-way ANOVA according to the following equation:

$$\mathrm{NFS}(m,t) = \mu(t) + \alpha(g,t) + \beta(s,t) + \gamma(h,t) + \epsilon(m,t) \quad (5)$$

where $\mu(t)$ is the overall climate response representing the grand ensemble mean of all projections at time t, $\alpha(g,t)$, $\beta(s,t)$ and $\gamma(h,t)$ are the main effects of GCM g, SDM s and HM h, respectively, and ϵ is the residual that may partly be due to model interactions. The empirical variances associated to these different effects correspond to the different components of model uncertainty – namely GCM, SDM, and HM uncertainty – and of residual/model interaction uncertainty, noted RMI in the following.

3.2.4 Partitioning internal variability

The internal climate variability variable η in Eq. (2) can be partitioned into a large scale and a small scale component. The first one originates from the internal/natural fluctuations of the climate and the latter results from the variability in local meteorological situations observed given a large scale atmospheric configuration. In the present multimember multimodel ensemble, the large scale internal variability (LSIV) stems from GCM internal variability. For a modeling chain driven by a given GCM, the LSIV leads to the fluctuations around the long term trend simulated with that chain. It also corresponds for any prediction lead time to the dispersion between projections obtained or that would be obtained for different runs of this GCM. The small scale internal variability (SSIV) originating here from a stochastic SDM is expressed as the deviations of the different stochastic realizations of a SDM for a given lead time.

For the present ensemble of projections, estimates of both internal variability components are derived with the quasi-ergodic assumption of transient climate simulations for relative change variables, following Appendix B of Hingray and Saïd (2014). This assumes that the variance of the studied variable – or more precisely the

HESSD
12, 12649–12701, 2015

coefficient of variation – is constant over the whole simulation period. In the present study, and conversely to the previous work, the baseline used for the estimation of the change variable is a constant $Y_0(m)$ that depends only on the modelling chain m. The expressions of SSIV(t) and LSIV(t) given by Hingray and Saïd (2014) thus simplify. They are given in Appendix A.

3.3 Application of the QE-ANOVA framework to low flows

3.3.1 Choice of NFS

Simple linear trend models are used to fit MAM7 projections of the whole period considered (1980–2065), on the contrary to Hingray and Saïd (2014) who considered piecewise NFSs composed of a constant value over a control period and a linear or polynomial trend over a transient period separated by a pivot year. The choice of a unique trend model is motivated by the shorter and wholly transient period considered here. Indeed, the pivot year has been estimated as 1950 and 1980 for temperature and precipitation respectively for the Durance@Serre-Ponçon by Hingray and Saïd (2014). The choice of a linear trend was made not to overfit large interannual fluctuations of the low flow indicator, as done by Hingray and Saïd (2014) for precipitation. The NFS are computed from 72 fitted linear trend models, one for each combination of GCM, SDM and hydrological model. Each NFS is then obtained by considering relative changes with respect to the average of the trend model for the associated chain over the 1980–2009 REF period following Eq. (4).

Figure 3 shows an example of winter low flow NFS for the Durance@Serre-Ponçon, for the IPCM4 GCM, the d2gen SDM, and the CLSM hydrological model. This specific NFS is a decrease reaching around −25 % in 2065 when the grand ensemble mean shows a much smaller decrease.

HESSD
12, 12649–12701, 2015

3.3.2 Extension of the framework to uncertainties in yearly anomalies

In this study, the QE-ANOVA framework is extended for partitioning the uncertainties not only on changes in time-slice averages as in the previous applications, but also on yearly anomalies of the raw values, in order to capture the effects of year-to-year variability in the uncertainty quantification. The studied variable Y in Eq. (2) is therefore taken as either y – the raw yearly variable – or $\overline{y}$ – a 30 year time-slice average. Uncertainty analyses on both yearly values and time-slice averages will be presented in parallel in the next section. It has to be noted that in both cases, NFSs are fitted to the yearly data, resulting in a similar decomposition of model uncertainties through the 3-way ANOVA.

4 Results

4.1 Identification of individual model effects

The 3-way ANOVA on NFSs (cf. Eq. 5) allows identifying individual model effects, i.e. average deviations of the NFSs from the grand ensemble mean μ due to a given model, be it a GCM, a SDM or a HM.

Figure 4 shows individual GCM effects around the grand ensemble mean. Looking first at this grand ensemble mean, low flows are projected to decrease in both catchments and in both seasons. However, when the decrease in 2065 is around only −7 % of the 1980–2009 average for the Durance in winter, it reaches −25 % in summer for both catchments and even exceeds −30 % in winter for the Verdon. The dispersion between GCM effects around the grand ensemble mean is quite large in winter, leading to changes ranging for example from −20 to +2 % for the Durance in 2065. The range of GCM effects is more limited in summer, but still higher than 10 % in 2065. CNCM33 (resp. ECHAM5) tends to systematically give a larger (resp. lower)

HESSD
12, 12649–12701, 2015

decrease than the grand ensemble mean. IPCM4 (resp. EGMAM2) also gives a larger (resp. lower) decrease, but only in summer.

Figure 5 shows individual SDM effects around the grand ensemble mean. Individual SDM effects are not homogeneous over catchments and seasons, with analog for example generating a stronger decrease for the Durance in winter and a smaller one for the Verdon in summer. In the other two situations, the dispersion between SDM effects is hardly noticeable.

Figure 6 shows individual hydrological model effects around the grand ensemble mean. The dispersion is here generally very large, with ranges of more than 30 % for the Durance in winter and for the Verdon in summer. The dispersion is more limited for the Verdon in winter. Looking into more details at individual models, ORCHIDEE stands as an outlier for the Durance in winter with a projected decrease of −28 % in 2065. Similarly, CLSM projects a much more severe decrease than other models in summer for both catchments. J2000 contrarily tends to generate a smaller decrease in all four cases.

4.2 Hierarchy of the different sources of uncertainty

The contribution of each source of uncertainty quantified by the QE-ANOVA approach can be expressed as a fraction of the total variance for each lead time t (see, e.g. Hawkins and Sutton, 2011). Figure 7 shows this decomposition of total variance for rolling 30 year average low flow changes in both catchments and both seasons. As expected, internal variability components contribute for the most part of the total variance for short lead times. They remain generally above 20 % in 2065 – and around 45 % for the Verdon in winter –, which is consistent with the analyses performed for the Durance by Hingray and Saïd (2014) on mean annual precipitation, and by Lafaysse et al. (2014) on mean annual streamflow. Large-scale internal variability accounts for around three quarters of the total internal variability, which is also consistent with previous studies. The decomposition of model uncertainty into GCM, SDM and HM contributions reveals interesting features: first, GCMs accounts for 15 to 25 % of the

HESSD
12, 12649–12701, 2015

total variance at the end of the period, and SDMs for less than 6 %, with even negligible contributions for the Verdon in winter and for the Durance in summer. The SDM contribution is thus much smaller than for the mean annual streamflow (see Lafaysse et al., 2014).

HM contribution to total variance is however largely non negligible. Values in 2065 reach 35 % in summer for both catchments and even 43 % for the Durance in winter. The Verdon in winter is the only case where values remain around 10 %. Lastly, residuals and model interactions generally account for 10 to 20 % of total variance.

Figure 8 shows a similar decomposition of total variance in both catchments and both seasons, but for yearly low flow anomalies. The most striking point is the very large contribution of internal variability components in all cases and for all lead times, up to more than 80 % in 2065, and even 94 % for the Verdon in winter. Such a prominence of internal variability is clearly visible in individual time series plots, even in Fig. 3, where the change signal of the considered NFS is yet rather high. Small-scale internal variability generally accounts here for one third of the total internal variability uncertainty. By construction of the NFSs, the remaining part of variance due to model uncertainties divides up into GCM, SDM, HM and residuals (RMI) in the same way as for time-slice averages in Fig. 7.

4.3 Projected evolution and associated confidence bounds

The total variance and grand ensemble mean computed through the QE-ANOVA approach allows deriving transient confidence bounds for the evolution of low flows, provided that an assumption is made on the shape of the distribution. Following previous uncertainty decomposition work on decadal averages, a normal distribution is selected for 30 year low flow averages (see, e.g. Hawkins and Sutton, 2009; Charlton-Perez et al., 2010; Hawkins and Sutton, 2011). A lognormal distribution is selected here for yearly values in order to take account of the skewed and bounded distribution of low flows. Additionally, confidence range may be partitioned into the different sources

HESSD
12, 12649–12701, 2015

of uncertainty identified by the QE-ANOVA approach in order to provide a transient evolution of these uncertainties.

Figure 9 shows the evolution of 30 year average changes in low flows and associated confidence bounds for both catchments and for both seasons. The total uncertainty increase with lead time in all cases and by a factor of 2.5 between 2009 and 2065 in summer, more than 3.5 for the Durance in winter, and only 1.3 for the Verdon in winter. The main contributor to this increase is HM uncertainty followed by GCM uncertainty. For the Verdon in winter, a decrease in both internal variability components nearly offsets this increase in model uncertainty.

Figure 10 plots the evolution of low flow yearly anomalies. The difference with respect to Fig. 9 lies in the amplitude of internal variability components. They moreover both tend to decrease with lead time as a consequence of the decrease in the grand ensemble mean. Their evolution counterbalances the increase in model uncertainties, leading to a reduction in total uncertainty in all cases except the Durance in winter.

4.4 Probability of a low flow decrease and potential to reduce uncertainty

Figure 9 suggests that the probability of a 30 year average low flow lower than the REF period average could be very close to 1 after 2050, except for the Durance in winter. Blue curves in Fig. 11 show the evolution of this probability along the period considered. Except for the Durance in winter where the change signal is too weak compared to uncertainties, the probability of a negative change between the REF period and a future period reaches 95 % in 2033–2039, that is for 30 year time-slices starting before 2015.

Red curves in Fig. 11 show the probability of a low flow for a given year being lower than the REF average. This second probability remains below 90 % even at the end of the period in all cases. It thus prevents to draw any definitive conclusion on the sign of the yearly anomaly with respect to the REF period average for any given lead time up to the end of the studied period.

The Time of Emergence (ToE) of the signal of change in average low flows is here determined in a transient way, more on the line with the approach of Hawkins and

HESSD
12, 12649–12701, 2015

Sutton (2012) than with recent hydrological applications in which it is only resolved at the 20 to 30 year time scale (see e.g. Köplin et al., 2014).

Figure 11 also shows the potential to reduce the uncertainty in low flow projections and more specifically its effect on the estimation of the probability of a low flow decrease. The potential to reduce uncertainty in projections is the part of total uncertainty due to models, i.e. the reducible part of this uncertainty (see Hawkins and Sutton, 2009, 2011). Dashed lines in Fig. 11 denote results that would be obtained with a perfect hydrometeorological model chain, by considering only uncertainties due to internal variability components and residuals, and assuming a unchanged grand ensemble mean response. Note that the latter assumption requires adopting a thruth-centered paradigm (see e.g. Knutti et al., 2010) for all model types, which is yet controversial for GCMs (see e.g. Sanderson and Knutti, 2012). The probability of a low flow decrease is of course higher in all cases. If little improvement is noted for yearly anomalies because of the large contribution of internal variability components, the time of emergence of the signal at the 95 % confidence level occurs around a decade earlier for both catchments in summer, and can be estimated at 2070 for the Durance in winter, where the signal is not expected to emerge with actual models.

5 Discussion

5.1 On the hydrological model uncertainty

Figure 7 highlighted the large and growing part of total uncertainty due to hydrological models on low flow projections in summer for both catchments, and in winter for the Durance. This part of uncertainty is higher than values obtained in other studies for other hydrological indicators like monthly flows (see e.g. Christierson et al., 2012; Bosshard et al., 2013). However, it is consistent with recent findings that HM uncertainty is higher than GCM uncertainty in snow-dominated catchments (see e.g. Giuntoli et al., 2015). Indeed, low flows are strongly linked to catchment processes

HESSD
12, 12649–12701, 2015

that may be represented differently in different hydrological models. It is therefore understandable that the contribution of HMs to the total uncertainty is higher than, say, for annual flood peak projections.

The fraction of variance due to the HMs in the whole ensemble of hydrological projections is checked against a simple single-time ANOVA decomposition approach proposed by von Storch and Zwiers (1999, chap. 9) and recently applied by Christierson et al. (2012) for a similar hydrology-climate partitioning purpose. The fraction of variance due to the HMs is estimated for each prediction lead time based on only data for that lead time, conversely to the time series approach of QE-ANOVA. It is computed as:

$$R_a^2 = \frac{\mathrm{SSA} - \frac{p-1}{p(n-1)}\mathrm{SSE}}{\mathrm{SST}} \quad (6)$$

where SSA is the treatment sum of squares, SSE the error sum of squares, SST the total sum of squares, p the number of HMs (6), and n the number of different climate projections used to force each HM (330). Figure 12 compares QE-ANOVA to the simpler approach for computing the fraction of variance explained by HMs for yearly low flow anomalies. Due to internal variability, estimates from the single-time approach are very noisy from one year to the next. QE-ANOVA results are quite consistent with this simpler approach and interestingly propose a smoother and more robust version of it. Figure 12 also shows a similar comparison for 30 year rolling averages and proposes similar conclusions, except that the noise in the simple approach estimates occur at the multidecadal time scale.

5.2 Origins of divergence in low flow responses from different hydrological models

After noticing this divergence in low flow responses to climate change from different hydrological models, one may ask about its origins in terms of physical processes.

HESSD
12, 12649–12701, 2015

Recall that for a given GCM-SDM chain – and a given run and stochastic realization of this chain – meteorological forcings are identical for all HMs. The only differences in hydrological effects thus originate from the physical parametrization of the HMs. The effects from individual models shown in Fig. 6 show that this divergence emerges from hydrological processes evolving differently in different models under a changed climate, all climate forcings being equal.

Computed summer low flows in snow-influenced catchments depend on two main factors other than external meteorological forcings: evapotranspiration and previous winter snowpack. More precisely, both Godsey et al. (2014) and Jenicek et al. (2015) suggested maximum Snow Water Equivalent (maxSWE) as a relevant predictor for summer minimum low flows.

Drivers of computed winter low flows are a bit harder to identify: indeed, winter low flows depend on the first hand on the timing of the snowpack building and melting, and therefore on rain/snow transition threshold and snowmelt parameters. On the other hand, they also depend on baseflow and therefore on evapotranspiration processes over the preceding months. Existing drought typologies as proposed by Van Loon and Van Lanen (2012) and Van Loon et al. (2015) may help in identifying potential drivers. Indeed, one way to consider a hydrological model leading to a higher than average low flow decrease is through its tendency to simulate more – with respect to the grand ensemble mean – hydrological droughts during one of the two low flow seasons in a changed climate. We use here the word hydrological drought for a streamflow deficit with respect to a daily variable threshold level as in Van Loon and Van Lanen (2012). In that specific sense, a drought is not necessarily associated with a severe low flow. Out of the 5 hydrological drought types identified by Van Loon et al. (2015) for cold climates, only 3 are therefore relevant for assessing winter low flows. On one hand, the Cold snow season drought and Warm snow season drought are closely related to the timing of snowpack building/melting, indicators of which are difficult to extract from time series (see e.g. Whitfield, 2013). On the other hand, Rain-to-sow-season drought describes the continuation of preceding water deficit into winter (see also Van Loon

HESSD
12, 12649–12701, 2015

et al., 2010). This deficit may be due to either a lack of precipitation – but this feature is not relevant here as total precipitation is a common forcing for all HMs – or to a strong evapotranspiration.

Based on all the above considerations, we selected two potential drivers of divergence in hydrological model responses: mean annual actual evapotranspiration (AET) and the maxSWE. We extracted AET and maxSWE output time series for all 1980 hydrological runs used in the low flow analysis above. Noise-free signals were extracted from these series in the same way than for low flows (see Sect. 3.2.2), and HM effects derived from these NFSs. Comparing HM effects on low flow changes with HM effects on AET/maxSWE may confirm possible drivers of the divergence, even if no causal relationship could be actually drawn.

Figure 13 first shows that effects on AET are negatively correlated with effects on low flows in both catchments and both seasons. Otherwise said, hydrological models showing a stronger increase in evaporation tend to simulate a stronger decrease in low flows. It is important to note that this somewhat reasonable relation is however not significant for summer flows at the 90 % confidence level. In summer, and for the Durance only, effects on low flows are significantly correlated with effects on the other potential driver (maxSWE). The slope of the relationship correspond to around 20 % of decrease in low flows for each 10 % decrease in maxSWE, which is quite consistent with findings from Godsey et al. (2014) on historical data in the Sierra Nevada (California). The relation between effects on low flows and effects on maxSWE for the Verdon in summer is not significant and has a gentler slope. This last result is again consistent with findings of Jenicek et al. (2015) who found a lower sensitivity of summer low flows to snow accumulation for less elevated catchments.

The interpretation of the positive (and significant) relation between effects on winter lows flows and effects on maxSWE is much more difficult. One would indeed expect on the contrary that storing less water in the snowpack would leave more water to sustain winter low flows. As mentioned above, winter low flows may originate from various and complex processes and some compensations may occur. Godsey et al.

HESSD
12, 12649–12701, 2015

(2014) indeed found that under a changed climate, a reduction in maxSWE may be offset by increased storage in autumn or winter and by shifts in the timing of maximum evapotranspiration. Moreover, both Magand et al. (2014) and Lafaysse et al. (2014) showed that a reduction in snow cover area leads to a higher evaporation on the Durance catchment. Further studies aiming at explaining the precise processes leading to a divergence in hydrological model responses on winter low flows should therefore explore these leads.

A way forward to disentangle the origins of the divergence in low flow responses from different hydrological models in general would be to make use of the Framework for Understanding Structural errors (FUSE Clark et al., 2008), which has already has been applied by Staudinger et al. (2011) to assess the performance on low flow indicators of a variety of model structures. Assessing the robustness of such structures in a climate change context would perhaps lead to improvements of existing model structure as those used in the present work.

5.3 Integrating additional sources of uncertainty

The hydrological projection dataset explored in this work includes a fairly comprehensive list of uncertainty types compared to most of previous studies (see Dobler et al., 2012; Addor et al., 2014, for recent hydrological studies with multiple uncertainty sources). However, some other potential sources of uncertainty were not considered. First, this dataset is conditional on the single A1B emissions scenario, which should not be detrimental to results presented above given the relatively close time horizon considered. Adding the scenario uncertainty in the QE-ANOVA framework would be relatively straightforward as it would take the form of an additional fixed effect alongside GCMs, SDMs and HMs.

Another potentially important contribution to the overall hydrological uncertainty would be the uncertainty in hydrological model parameters. The time transferability of model parameters in a climate change context and its contribution to overall uncertainties has recently been explored by some studies (see e.g. Finger et al., 2012;

HESSD
12, 12649–12701, 2015

Dobler et al., 2012). One way to incorporate this source of uncertainty into the QE-ANOVA framework and combine it with hydrological model structure uncertainty would be to devise a calibration protocol common to all HMs that would split the calibration period into distinct subperiods showing climatic contrasts, as proposed and applied by Thirel et al. (2015). Such a protocol has actually already been applied in the R2D2-2050 project (see Sauquet et al., 2014) for a subset of hydrological model structures and the analysis of results will be the subject of a follow-up paper. Results based on CLSM for a small upstream Durance subcatchment showed that hydrological projections may be highly sensitive to the calibration period through some specific parameterized processes (Magand et al., 2015). Using such a calibration protocol may then allow computing the hydrological model parameter contribution in a way similar to internal climate variability components in the QE-ANOVA framework.

6 Conclusions

This paper proposes a methodology for estimating the transient probability distribution of yearly hydrological variables conditional to an ensemble of projections built from multiple general circulation models (GCMs), multiple statistical downscaling methods (SDMs) and multiple hydrological models (HMs). The methodology is based on the quasi-ergodic analysis of variance (QE-ANOVA) framework that allows quantifying the contributions of the different sources of total uncertainty, by critically taking account of (1) large-scale internal variability stemming from the transient evolution of multiple GCM runs, and (2) small-scale internal variability derived from multiple realizations of stochastic SDMs. The QE-ANOVA framework was initially developed for long-term climate averages and is here extended to include year-to-year climate variability in probabilistic hydrological projections, thereby following the recommendations of Sexton and Harris (2015). Indeed, results from climate impact and adaptation projects usually focus on time-slice changes, and therefore underestimate the role of climate variability. Taking account of the year-to-year variability which is large for hydrological variables

HESSD
12, 12649–12701, 2015

in general – and for low flows in particular – is therefore especially relevant for better informing water resource adaptation strategies. To the authors' knowledge, it is the first time that a transient quantification of low flow uncertainties (including internal variability) is proposed.

The QE-ANOVA framework is applied to better understand possible transient futures of both winter and summer low flows for two snow-influenced catchments in the southern French Alps. The analysis takes advantage of a very large dataset of daily transient hydrological projections over the 1981–2065 period, that combines in a comprehensive way 11 runs from 4 different GCMs, 3 SDMs with 10 stochastic realizations each, as well as 6 diverse HMs. Results from the extended QE-ANOVA approach may be summarized into three points. First, the change signal is a decrease in yearly low flows of around −20 % in 2065 with respect to the 1980–2009 reference, except for the most elevated catchment in winter where low flows barely decrease. Second, this change signal of yearly low flow anomalies is largely masked by both large- and small-scale internal variability, even in 2065 at the end of the period considered. The time of emergence of the change signal on 30 year low-flow averages is however around 2035, i.e. for time slices starting in 2020. But the most striking result is that a large part of the total uncertainty – up to 40 % in 2065 for 30 year averages compared to less than 25 % due to the GCMs – stems from the difference in hydrological model responses.

Two main conclusions can be drawn from the above analysis, leading to corresponding lessons for future actions. First, internal variability brings by far the largest part of the uncertainty in low flows for an individual year in the future, even when the change signal is relatively large. From the water manager point of view, the best way to adapt to climate change would therefore be to adapt to climate variability. The scientific focus should then be on providing robust estimates of this internal climate variability by for example looking more and further into the past to identify benchmark situations and events that would serve as training sets for testing adaptation strategies.

HESSD
12, 12649–12701, 2015

Second, low flow responses from different hydrological models diverge in a changing climate, presumably due to differences in both evapotranspiration and snowpack components resulting from the large range of approaches implemented in the 6 hydrological models used here. Hydrological models should therefore be carefully checked for their robustness in a changed climate in order to increase the confidence in hydrological projections. In particular, efforts should be put on validating the robustness of all components of hydrological models with specific analyses and relevant datasets, notably for evapotranspiration and snowpack evolution.

Appendix A: Expressions of internal variability components

A1 Small scale internal variability

When a single GCM run is available for a given modelling chain m, the small-scale internal variability component of Δ for m can be estimated for any future prediction lead time t from the empirical inter-realization variance of Δ for t (Eq. B2 in Hingray and Saïd, 2014). In the present work, the reference used for the estimation of the change variable is a constant (namely $Y_0(m)$). The expression thus simplifies as:

$$\mathrm{Var}_k(\Delta) \approx \left(\frac{\hat{y}(m,t)}{Y_0(m)}\right)^2 \cdot \mathrm{Var}_k\left[\frac{Y(m,r,k,t)}{\hat{y}(m,t)}\right] \quad \text{(A1)}$$

where Var_k is the empirical variance over stochastic realizations.

The variance in Eq. (A1) is equivalent to a coefficient of variation of Y with respect to the inter-realization variance. Assuming this coefficient of variation as roughly constant over the whole simulation period, the SSIV of chain m may be thus estimated from the temporal mean of this coefficient for this specific chain. When multiple runs are available for m, the SSIV of Δ for m is estimated from the multirun mean of their temporal mean. The SSIV component for the whole projection ensemble is finally

HESSD
12, 12649–12701, 2015

derived for each lead time t as the multichain mean of these chain-specific estimates:

$$\mathrm{SSIV}(t) \approx \frac{1}{N_g N_s N_h} \sum_{g=1}^{N_g} \sum_{s=1}^{N_s} \sum_{h=1}^{N_h} \frac{1}{T N_{g,r}} \left(\frac{\hat{y}(m,t)}{Y_0(m)} \right)^2 \cdot \sum_{r=1}^{N_{g,r}} \sum_{t=1}^{T} \mathrm{Var}_k \left[\frac{Y(m,r,k,t)}{\hat{y}(m,t)} \right] \quad \text{(A2)}$$

where T is the total number of time steps covered by the simulation period and $N_{g,r}$ is the number of runs for GCM g. Note that the SSIV is a function of time via the signal terms $\hat{y}(m,t)$ in Eqs. (A1) and (A2).

A2 Large scale internal variability

The large scale internal variability component for any given chain m has the same expression as that of SSIV in Eq. (A1) but, due to the limited number of runs available, the inter-run variance (or equivalently the coefficient of variation) cannot be estimated in a robust way. Following the quasi-ergodic assumption for transient climate projections, the LSIV for Y with respect to the inter-run dispersion is assumed to be, in terms of coefficient of variation, constant over the whole simulation period. It follows that for any time t and any chain m:

$$\mathrm{Var}_r \left(\frac{Y(m,r,\bullet,t)}{\hat{y}(m,t)} \right) \approx \mathrm{Var}_T \left(\frac{Y(m,r,\bullet,t)}{\hat{y}(m,t)} \right). \quad \text{(A3)}$$

where Var_r is the empirical variance over runs, Var_T is the empirical variance over time, and $Y(m,r,\bullet,t)$ denotes the average over all stochastic realizations from SDM s.

When multiple runs are available for a chain, this variance component is estimated from all runs. The LSIV component of Δ is finally estimated from the multimodel mean of the temporal and inter-run variance of $Y(m,r,\bullet,t)$ (Eq. B6 in Hingray and Saïd, 2014). Again, as the reference used here for estimating relative changes is a constant, the

HESSD
12, 12649–12701, 2015

expression simplifies as:

$$\mathrm{LSIV}(t) = \frac{1}{N_g N_s N_h} \sum_{g=1}^{N_g} \sum_{s=1}^{N_s} \sum_{h=1}^{N_h} \left(\frac{\hat{y}(m,t)}{Y_0(m)} \right)^2 \cdot \mathrm{Var}_{T,N_{g,r}} \left(\frac{Y(m,r,\bullet,t)}{\hat{y}(m,t)} \right) \quad \text{(A4)}$$

Acknowledgements. This work was supported by funding from the French Department in charge of the Environment through the R2D2-250 project. Analyses were performed in R (R Development Core Team, 2014), with packages `lfstat` (Koffler and Lahaa, 2014), `tidyr` (Wickham, 2014a, b), `dplyr` (Wickham and François, 2015), `ggplot2` (Wickham, 2009, 2011), `RColorBrewer` (Neuwirth, 2014), `RcppRoll` (Ushey, 2015) and `fitdistrplus` (Delignette-Muller and Dutang, 2015). All authors thank participants from various partner institutions in the R2D2-2050 project that contributed their modelling outputs to the hydrological projection dataset used here: Céline Monteil (EDF R&D), Frédéric Hendrickx (EDF R&D), Marie Bourqui (now at EDF DTG), Thibault Mathevet (EDF DTG), Matthieu Le Lay (EDF DTG), Joël Gailhard (EDF DTG), Matthieu Lafaysse (now at CNRM-CEN), Abdelkader Mezghani (now at Met.No) Flora Branger (Irstea HHLY), François Tilmant (Irstea HHLY), Guillaume Thirel (Irstea HBAN) and Charles Perrin (Irstea HBAN).

References

Addor, N., Rössler, O., Köplin, N., Huss, M., Weingartner, R., and Seibert, J.: Robust changes and sources of uncertainty in the projected hydrological regimes of Swiss catchments, Water Resour. Res., 50, 7541–7562, doi:10.1002/2014WR015549, 2014. 12652, 12670

Allen, R. G., Pereira, L. S., Raes, D., and Smith, M.: Crop Evapotranspiration – Guidelines for computing crop water requirements, FAO Irrigation and Drainage Paper 56, FAO, Rome, 1998. 12656

Barria, P., Walsh, K. J. E., Peel, M. C., and Karoly, D.: Uncertainties in runoff projections in southwestern Australian catchments using a global climate model with perturbed physics, J. Hydrol., 529, 184–199, doi:10.1016/j.jhydrol.2015.07.040, 2015. 12652

Boé, J., Terray, L., Habets, F., and Martin, E.: A simple statistical-dynamical downscaling scheme based on weather types and conditional resampling, J. Geophys. Res., 111, D23106, doi:10.1029/2005JD006889, 2006. 12687

HESSD
12, 12649–12701, 2015

Boé, J., Terray, L., Martin, E., and Habets, F.: Projected changes in components of the hydrological cycle in French river basins during the 21st century, Water Resour. Res., 45, W08426, doi:10.1029/2008WR007437, 2009. 12656

Bosshard, T., Carambia, M., Goergen, K., Kotlarski, S., Krahe, P., Zappa, M., and Schär, C.: Quantifying uncertainty sources in an ensemble of hydrological climate-impact projections, Water Resour. Res., 49, 1523–1536, doi:10.1029/2011WR011533, 2013. 12652, 12666

Bourqui, M., Mathevet, T., Gailhard, J., and Hendrickx, F.: Hydrological validation of statistical downscaling methods applied to climate model projections, in: Hydro-climatology: Variability and Change, edited by: Franks, S. W., Boegh, E., Blyth, E., Hannah, D. M., and Yilmaz, K. K., AISH, Wallingford, UK, IAHS-AISH Red Books, 344, 33–38, 2011. 12655, 12657

Bracegirdle, T. J., Turner, J., Hosking, J. S., and Phillips, T.: Sources of uncertainty in projections of twenty-first century westerly wind changes over the Amundsen Sea, West Antarctica, in CMIP5 climate models, Clim. Dynam., 43, 2093–2104, doi:10.1007/s00382-013-2032-1, 2014. 12659

Bréthaut, C. and Hill Clarvis, M.: Interdisciplinary approaches for analysing governance challenges across the Rhône basin, Reg. Environ. Change, 15, 499–503, doi:10.1007/s10113-014-0747-0, 2015. 12651, 12654

Charlton-Perez, A. J., Hawkins, E., Eyring, V., Cionni, I., Bodeker, G. E., Kinnison, D. E., Akiyoshi, H., Frith, S. M., Garcia, R., Gettelman, A., Lamarque, J. F., Nakamura, T., Pawson, S., Yamashita, Y., Bekki, S., Braesicke, P., Chipperfield, M. P., Dhomse, S., Marchand, M., Mancini, E., Morgenstern, O., Pitari, G., Plummer, D., Pyle, J. A., Rozanov, E., Scinocca, J., Shibata, K., Shepherd, T. G., Tian, W., and Waugh, D. W.: The potential to narrow uncertainty in projections of stratospheric ozone over the 21st century, Atmos. Chem. Phys., 10, 9473–9486, doi:10.5194/acp-10-9473-2010, 2010. 12659, 12664

Chauveau, M., Chazot, S., Perrin, C., Bourgin, P.-Y., Sauquet, E., Vidal, J.-P., Rouchy, N., Martin, E., David, J., Norotte, T., Maugis, P., and de Lacaze, X.: What will be the impacts of climate change on surface hydrology in France by 2070?, Houille Blanche, 4, 5–15, doi:10.1051/lhb/2013027, 2013. 12651, 12655, 12657

Christierson, B. v., Vidal, J.-P., and Wade, S. D.: Using UKCP09 probabilistic climate information for UK water resource planning, J. Hydrol., 424–425, 48–67, doi:10.1016/j.jhydrol.2011.12.020, 2012. 12651, 12656, 12666, 12667

Clark, M. P., Slater, A. G., Rupp, D. E., Woods, R. A., Vrugt, J. A., Gupta, H. V., Wagener, T., and Hay, L. E.: Framework for Understanding Structural Errors (FUSE): a modular framework

HESSD
12, 12649–12701, 2015

to diagnose differences between hydrological models, Water Resour. Res., 44, W00B02, doi:10.1029/2007WR006735, 2008. 12670
Clarvis, M. H., Fatichi, S., Allan, A., Fuhrer, J., Stoffel, M., Romerio, F., Gaudard, L., Burlando, P., Beniston, M., and Xoplaki, E. Toreti, A.: Governing and managing water resources under changing hydro-climatic contexts: the case of the upper Rhone basin, Environ. Sci. Policy, 43, 56–67, doi:10.1016/j.envsci.2013.11.005, 2014. 12651
Delignette-Muller, M. L. and Dutang, C.: fitdistrplus: An R package for fitting distributions, J. Stat. Softw., 64, 1–34, 2015. 12675
Deser, C., Phillips, A., Bourdette, V., and Teng, H.: Uncertainty in climate change projections: the role of internal variability, Clim. Dynam., 38, 527–546, doi:10.1007/s00382-010-0977-x, 2012. 12652
Dobler, C., Hagemann, S., Wilby, R. L., and Stötter, J.: Quantifying different sources of uncertainty in hydrological projections in an Alpine watershed, Hydrol. Earth Syst. Sci., 16, 4343–4360, doi:10.5194/hess-16-4343-2012, 2012. 12652, 12670, 12671
Ducharne, A., Koster, R. D., Suarez, M. J., Stieglitz, M., and Kumar, P.: A catchment-based approach to modeling land surface processes in a general circulation model 2. Parameter estimation and model demonstration, J. Geophys. Res., 105, 24823–24838, doi:10.1029/2000JD900328, 2000. 12688
Etchevers, P., Golaz, C., Habets, F., and Noilhan, J.: Impact of a climate change on the Rhone river catchment hydrology, J. Geophys. Res., 107, ACL 6-1–ACL 6-18, doi:10.1029/2001JD000490, 2002. 12656
Fatichi, S., Rimkus, S., Burlando, P., Bordoy, R., and Molnar, P.: High-resolution distributed analysis of climate and anthropogenic changes on the hydrology of an Alpine catchment, J. Hydrol., 525, 362–382, doi:10.1016/j.jhydrol.2015.03.036, 2015. 12652
Finger, D., Heinrich, G., Gobiet, A., and Bauder, A.: Projections of future water resources and their uncertainty in a glacierized catchment in the Swiss Alps and the subsequent effects on hydropower production during the 21st century, Water Resour. Res., 48, W02521, doi:10.1029/2011WR010733, 2012. 12652, 12670
Garçon, R.: Overall rain-flow model for flood forecasting and pre-determination, Houille Blanche, 54, 88–95, doi:10.1051/lhb/1999088, 1999. 12688
Gelfan, A., Semenov, V. A., Gusev, E., Motovilov, Y., Nasonova, O., Krylenko, I., and Kovalev, E.: Large-basin hydrological response to climate model outputs: uncertainty caused by internal

HESSD
12, 12649–12701, 2015

atmospheric variability, Hydrol. Earth Syst. Sci., 19, 2737–2754, doi:10.5194/hess-19-2737-2015, 2015. 12652

Giuntoli, I., Vidal, J.-P., Prudhomme, C., and Hannah, D. M.: Future hydrological extremes: the uncertainty from multiple global climate and global hydrological models, Earth Syst. Dynam., 6, 267–285, doi:10.5194/esd-6-267-2015, 2015. 12652, 12666

Godsey, S. E., Kirchner, J. W., and Tague, C. L.: Effects of changes in winter snowpacks on summer low flows: case studies in the Sierra Nevada, California, USA, Hydrol. Process., 28, 5048–5064, doi:10.1002/hyp.9943, 2014. 12668, 12669

Gottardi, F., Obled, C., Gailhard, J., and Paquet, E.: Statistical reanalysis of precipitation fields based on ground network data and weather patterns: Application over French mountains, J. Hydrol., 432–433, 154–167, doi:10.1016/j.jhydrol.2012.02.014, 2012. 12656, 12689

Green, M. and Weatherhead, E. K.: The application of probabilistic climate change projections: a comparison of methods of handling uncertainty applied to UK irrigation reservoir design, Journal of Water and Clim. Change, 5, 652–666, doi:10.2166/wcc.2014.125, 2014. 12656

Habets, F., Boé, J., Déqué, M., Ducharne, A., Gascoin, S., Hachour, A., Martin, E., Pagé, C., Sauquet, E., Terray, L., Thiéry, D., Oudin, L., and Viennot, P.: Impact of climate change on the hydrogeology of two basins in northern France, Climatic Change, 121, 771–785, doi:10.1007/s10584-013-0934-x, 2013. 12657

Hagemann, S., Chen, C., Clark, D. B., Folwell, S., Gosling, S. N., Haddeland, I., Hanasaki, N., Heinke, J., Ludwig, F., Voss, F., and Wiltshire, A. J.: Climate change impact on available water resources obtained using multiple global climate and hydrology models, Earth Syst. Dynam., 4, 129–144, doi:10.5194/esd-4-129-2013, 2013. 12652

Hawkins, E. and Sutton, R.: The potential to narrow uncertainty in regional climate predictions, B. Am. Meteorol. Soc., 90, 1095–1107, doi:10.1175/2009BAMS2607.1, 2009. 12652, 12664, 12666

Hawkins, E. and Sutton, R.: The potential to narrow uncertainty in projections of regional precipitation change, Clim. Dynam., 37, 407–418, doi:10.1007/s00382-010-0810-6, 2011. 12652, 12663, 12664, 12666, 12697

Hawkins, E. and Sutton, R.: Time of emergence of climate signals, Geophys. Res. Lett., 39, L01702, doi:10.1029/2011GL050087, 2012. 12665

Hendrickx, F.: Impact of climate change on the hydrology of the Rhône catchment, Hydroécologie Appliquée, 13, 77–100, doi:10.1051/hydro:2001007, 2001. 12688

HESSD

12, 12649–12701, 2015

Hingray, B. and Saïd, M.: Partitioning internal variability and model uncertainty components in a multimodel multireplicate ensemble of climate projections, J. Climate, 27, 6779–6798, doi:10.1175/JCLI-D-13-00629.1, 2014. 12653, 12655, 12658, 12660, 12661, 12663, 12673, 12674, 12697

Hingray, B., Hendrickx, F., Bourqui, M., Creutin, J.-D., François, B., Gailhard, J., Lafaysse, M., Lemoine, N., Mathevet, T., Mezghani, A., and Monteil, C.: RIWER2030. Climat Régionaux et Incertitudes, Ressource en Eau et Gestion associée de 1860 à 2100, Final report, ANR, Grenoble, France, 2013. 12655, 12656

Huebener, H., Cubasch, U., Langematz, U., Spangehl, T., Niehörster, F., Fast, I., and Kunze, M.: Ensemble climate simulations using a fully coupled ocean-troposphere–stratosphere general circulation model, Philos. T. Roy. Soc. A, 365, 2089–2101, doi:10.1098/rsta.2007.2078, 2007. 12686

Jenicek, M., Seibert, J., Zappa, M., Staudinger, M., and Jonas, T.: Importance of maximum snow accumulation for summer low flows in humid catchments, Hydrol. Earth Syst. Sci. Discuss., 12, 7023–7056, doi:10.5194/hessd-12-7023-2015, 2015. 12668, 12669

Johns, T. C., Royer, J.-F., Höschel, I., Huebener, H., Roeckner, E., Manzini, E., May, W., Dufresne, J.-L., Otterå, O. H., van Vuuren, D. P., Salas y Melia, D., Giorgetta, M. A., Denvil, S., Yang, S., Fogli, P. G., Körper, J., Tjiputra, J. F., Stehfest, E., and Hewitt, C. D.: Climate change under aggressive mitigation: the ENSEMBLES multi-model experiment, Clim. Dynam., 37, 1975–2003, doi:10.1007/s00382-011-1005-5, 2011. 12655

Kalnay, E., Kanamitsu, M., Kistler, R., W., C., Deaven, D., Gandin, L., Iredell, M., Saha, S., White, G., Woollen, J., Zhu, Y., Chelliah, M., Ebisuzaki, W., Higgins, W., Janoviak, J., Mo, K. C., Ropelewski, C., Wang, J., Leetmaa, A., Reynolds, R., Jenne, R., and Joseph, D.: The NCEP/NCAR 40-year Reanalysis Project, B. Am. Meteorol. Soc., 77, 437–471, doi:10.1175/1520-0477(1996)077<0437:TNYRP>2.0.CO;2, 1996. 12656

Knutti, R., Furrer, R., Tebaldi, C., Cermak, J., and Meehl, G. A.: Challenges in combining projections from multiple climate models, J. Climate, 23, 2739–2758, doi:10.1175/2009JCLI3361.1, 2010. 12666

Koffler, D. and Lahaa, G.: lfstat: Calculation of Low Flow Statistics for daily stream flow data, R package version 0.6, 2014. 12675

Köplin, N., Rößler, O., Schädler, B., and Weingartner, R.: Robust estimates of climate-induced hydrological change in a temperate mountainous region, Climatic Change, 122, 171–184, doi:10.1007/s10584-013-1015-x, 2014. 12666

HESSD
12, 12649–12701, 2015

Krause, P.: Quantifying the impact of land use changes on the water balance of large catchments using the J2000 model, Phys. Chem. Earth, 27, 663–673, doi:10.1016/S1474-7065(02)00051-7, 2002. 12688

Krinner, G., Viovy, N., de Noblet-Ducoudré, N., Ogée, J., Polcher, J., Friedlingstein, P., Ciais, P., Sitch, S., and Prentice, I. C.: A dynamic global vegetation model for studies of the coupled atmosphere–biosphere system, Global Biogeochem. Cy., 19, GB1015, doi:10.1029/2003GB002199, 2005. 12688

Laaha, G. and Blöschl, G.: A comparison of low flow regionalisation methods–catchment grouping, J. Hydrol., 323, 193–214, doi:10.1016/j.jhydrol.2005.09.001, 2006a. 12657

Laaha, G. and Blöschl, G.: Seasonality indices for regionalizing low flows, Hydrol. Process., 20, 3851–3878, doi:10.1002/hyp.6161, 2006b. 12657

Laaha, G., Demuth, S., Hisdal, H., Kroll, C. N., van Lanen, H. A. J., Nester, T., Rogger, M., Sauquet, E., Tallaksen, L. M., Woods, R., and Young, A.: Prediction of low flows in ungauged basins, in: Runoff Prediction in Ungauged Basins – Synthesis across Processes, Places and Scales, edited by: Blöschl, G., Sivapalan, M., Wagener, T., Viglione, A., and Savenije, H., Cambridge University Press, Cambridge, UK, chap. 8, 163–188, 2013. 12657

Lafaysse, M., Hingray, B., Terray, L., Mezghani, A., and Gailhard, J.: Internal variability and model uncertainty components in future hydrometeorological projections: the Alpine Durance basin, Water Resour. Res., 50, 3317–3341, doi:10.1002/2013WR014897, 2014. 12652, 12655, 12658, 12663, 12664, 12670

Lorenz, E. N.: Atmospheric predictability as revealed by naturally occurring analogues, J. Atmos. Sci., 26, 636–646, doi:10.1175/1520-0469(1969)26<636%3AAPARBN>2.0.CO%3B2, 1969. 12655

Magand, C., Ducharne, A., Le Moine, N., and Gascoin, S.: Introducing hysteresis in snow depletion curves to improve the water budget of a land surface model in an Alpine catchment, J. Hydrometeorol., 15, 631–649, doi:10.1175/JHM-D-13-091.1, 2014. 12656, 12670

Magand, C., Ducharne, A., Le Moine, N., and Brigode, P.: Parameter transferability under changing climate: case study with a land surface model in the Durance watershed, France, Hydrolog. Sci. J., 60, 1408–1423, doi:10.1080/02626667.2014.993643, 2015. 12671

Marti, O., Braconnot, P., Dufresne, J.-L., Bellier, J., Benshila, R., Bony, S., Brockmann, P., Cadule, P., Caubel, A., Codron, F., de Noblet, N., Denvil, S., Fairhead, L., Fichefet, T., Foujols, M.-A., Friedlingstein, P., Goosse, H., Grandpeix, J.-Y., Guilyardi, E., Hourdin, F.,

HESSD
12, 12649–12701, 2015

Idelkadi, A., Kageyama, M., Krinner, G., Lévy, C., Madec, G., Mignot, J., Musat, I., Swingedouw, D., and Talandier, C.: Key features of the IPSL ocean atmosphere model and its sensitivity to atmospheric resolution, Clim. Dynam., 34, 1–26, doi:10.1007/s00382-009-0640-6, 2010. 12686

McKay, M. D., Beckman, R. J., and Conover, W. J.: A comparison of three methods for selecting values of input variables in the analysis of output from a computer code, Technometrics, 21, 239–245, doi:10.2307/1268522, 1979. 12656

Mezghani, A. and Hingray, B.: A combined downscaling-disaggregation weather generator for stochastic generation of multisite hourly weather variables over complex terrain: development and multi-scale validation for the Upper Rhone River basin, J. Hydrol., 377, 245–260, doi:10.1016/j.jhydrol.2009.08.033, 2009. 12656, 12687

Minasny, B. and McBratney, A. B.: A conditioned Latin hypercube method for sampling in the presence of ancillary information, Comput. Geosci., 32, 1378–1388, doi:10.1016/j.cageo.2005.12.009, 2006. 12656

Moatar, F., Ducharne, A., Thiéry, D., Bustillo, V., Sauquet, E., and Vidal, J.-P.: La Loire à l'épreuve du changement climatique, Géosciences, 12, 79–87, 2010. 12657

Murphy, J. M., Sexton, D. M. H., Jenkins, G. J., Booth, B. B. B., Brown, C. C., Clark, R. T., Collins, M., Harris, G. R., Kendon, E. J., Betts, R. A., Brown, S. J., Humphrey, K. A., McCarthy, M. P., McDonald, R. E., Stephens, A., Wallace, C., Warren, R., Wilby, R., and Wood, R. A.: Climate change projections, UK climate projections science report, Met Office Hadley Centre, Exeter, 2009. 12656

Nakićenović, N., Alcamo, J., Davis, G., de Vries, B., Fenhann, J., Gaffin, S., Gregory, K., Grübler, A., Jung, T. Y., Kram, T., La Rovere, E. L., Michaelis, L., Mori, S., Morita, T., Pepper, W., Pitcher, H., Price, L., Riahi, K., Roehrl, A., Rogner, H.-H., Sankovski, A., Schlesinger, M., Shukla, P., Smith, S., Swart, R., van Rooijen, S., Victor, N., and Dadi, Z.: Special Report on Emissions Scenarios, Cambridge University Press, Intergovernmental Panel on Climate Change, IPCC, 2000. 12655

Neuwirth, E.: RColorBrewer: ColorBrewer Palettes, R package version 1.1-2, 2014. 12675

Obled, C., Bontron, G., and Garçon, R.: Quantitative precipitation forecasts: a statistical adaptation of model outputs through an analogues sorting approach, Atmos. Res., 63, 303–324, doi:10.1016/S0169-8095(02)00038-8, 2002. 12687

Paiva, R., Collischonn, W., Schnetterling, E. B., Vidal, J.-P., Hendrickx, F., and Lopez, A.: The case studies, in: Modelling the Impact of Climate Change on Water Resources, edited by:

HESSD
12, 12649–12701, 2015

Fung, F., Lopez, A., and New, M., John Wiley & Sons, Ltd, Chichester, UK, chap. 6, 136–182, doi:10.1002/9781444324921.ch6, 2010. 12657
Peel, M. C., Srikanthan, R., McMahon, T. A., and Karoly, D. J.: Approximating uncertainty of annual runoff and reservoir yield using stochastic replicates of global climate model data, Hydrol. Earth. Syst. Sc., 19, 1615–1639, doi:10.5194/hess-19-1615-2015, 2015. 12652
Pushpalatha, R., Perrin, C., Le Moine, N., Mathevet, T., and Andréassian, V.: A downward structural sensitivity analysis of hydrological models to improve low-flow simulation, J. Hydrol., 411, 66–76, doi:10.1016/j.jhydrol.2011.09.034, 2011. 12688
R Development Core Team: R: A Language and Environment for Statistical Computing, R Foundation for Statistical Computing, Vienna, Austria, ISBN 3-900051-07-0, 2014. 12675
Roeckner, E., Giorgetta, M. A., Crueger, T., Esch, M., and Pongratz, J.: Sensitivity of simulated climate to horizontal and vertical resolution in the ECHAM5 atmosphere model, J. Climate, 19, 3771–3791, doi:10.1175/JCLI3824.1, 2006. 12686
Salas-Mélia, D., Chauvin, F., Déqué, M., Douville, H., Guérémy, J.-F., Marquet, P., Planton, S., Royer, J.-F., and Tyteca, S.: Description and validation of the CNRM-CM3 global coupled model, CNRM Working Note 103, CNRM-GAME, Toulouse, France, 2005. 12686
Sanderson, B. M. and Knutti, R.: On the interpretation of constrained climate model ensembles, Geophys. Res. Lett., 39, L16708, doi:10.1029/2012GL052665, 2012. 12666
Sansom, P. G., Stephenson, D. B., Ferro, C. A. T., Zappa, G., and Shaffrey, L.: Simple uncertainty frameworks for selecting weighting schemes and interpreting multi-model ensemble climate change experiments, J. Climate, 26, 4017–4037, doi:10.1175/JCLI-D-12-00462.1, 2013. 12652
Sauquet, E., Arama, Y., Blanc-Coutagne, E., Bouscasse, H., Branger, F., Braud, I., Brun, J.-F., Chérel, Y., Cipriani, T., Datry, T., Ducharne, A., Hendrickx, F., Hingray, B., Krowicki, F., Le Goff, I., Le Lay, M., Magand, C., Malerbe, F., Mathevet, T., Monteil, C., Perrin, C., Poulhe, P., Rossi, A., Samie, R., Strosser, P., Thirel, G., Tilmant, F., and Vidal, J.-P.: Risk, water Resources and sustainable Development within the Durance river basin in 2050, Final Report 10-GCMOT-GICC-3-CVS-102, MEDDE, Villeurbanne, France, 2014. 12654, 12671
Schewe, J., Heinke, J., Gerten, D., Haddeland, I., Arnell, N. W., Clark, D. B., Dankers, R., Eisner, S., Fekete, B. M., Colón-González, F. J., Gosling, S. N., Kim, H., Liu, X., Masaki, Y., Portmann, F. T., Satoh, Y., Stacke, T., Tang, Q., Wada, Y., Wisser, D., Albrecht, T., Frieler, K., Piontek, F., Warszawski, L., and Kabat, P.: Multimodel assessment of water scarcity under

HESSD
12, 12649–12701, 2015

climate change, P. Natl. Acad. Sci. USA, 111, 3245–3250, doi:10.1073/pnas.1222460110, 2014. 12652

Seiller, G. and Anctil, F.: Climate change impacts on the hydrologic regime of a Canadian river: comparing uncertainties arising from climate natural variability and lumped hydrological model structures, Hydrol. Earth Syst. Sci., 18, 2033–2047, doi:10.5194/hess-18-2033-2014, 2014. 12652

Sexton, D. M. H. and Harris, G. R.: The importance of including variability in climate change projections used for adaptation, Nature Clim. Change, 5, 931–936, doi:10.1038/nclimate2705, 2015. 12651, 12671

Staudinger, M., Stahl, K., Seibert, J., Clark, M. P., and Tallaksen, L. M.: Comparison of hydrological model structures based on recession and low flow simulations, Hydrol. Earth Syst. Sci., 15, 3447–3459, doi:10.5194/hess-15-3447-2011, 2011. 12670

Thirel, G., Andréassian, V., Perrin, C., Audouy, J.-N., Berthet, L., Edwards, P., Folton, N., Furusho, C., Kuentz, A., Lerat, J., Lindström, G., Martin, E., Mathevet, T., Merz, R., Parajka, J., Ruelland, D., and Vaze, J.: Hydrology under change: an evaluation protocol to investigate how hydrological models deal with changing catchments, Hydrolog. Sci. J., 60, 1184–1199, doi:10.1080/02626667.2014.967248, 2015. 12671

Ushey, K.: RcppRoll: Efficient Rolling/Windowed Operations, R package version 0.2.2, 2015. 12675

van der Linden, P. and Mitchell, J. F. B.: ENSEMBLES: Climate Change and its Impacts: Summary of research and results from the ENSEMBLES project, Tech. rep., Met Office Hadley Centre, 2009. 12655

Van Loon, A. F. and Van Lanen, H. A. J.: A process-based typology of hydrological drought, Hydrol. Earth Syst. Sci., 16, 1915–1946, doi:10.5194/hess-16-1915-2012, 2012. 12668

Van Loon, A. F., Van Lanen, H. A. J., Hisdal, H., Tallaksen, L. M., Fendeková, M., Oosterwijk, J., Horvát, O., and Machlica, A.: Understanding hydrological winter drought in Europe, in: Global Change: Facing Risks and Threats to Water Resources, edited by: Servat, E., Demuth, S., Dezetter, A., and Daniell, T., IAHS, Wallingford, UK, IAHS Red Books, 340, 189–197, 2010. 12668

Van Loon, A. F., Ploum, S. W., Parajka, J., Fleig, A. K., Garnier, E., Laaha, G., and Van Lanen, H. A. J.: Hydrological drought types in cold climates: quantitative analysis of causing factors and qualitative survey of impacts, Hydrol. Earth Syst. Sci., 19, 1993–2016, doi:10.5194/hess-19-1993-2015, 2015. 12668

HESSD

12, 12649–12701, 2015

van Pelt, S. C. and Beersma, J. J., Buishand, T. A., van den Hurk, B. J. J. M., and Schellekens, J.: Uncertainty in the future change of extreme precipitation over the Rhine basin: the role of internal climate variability, Clim. Dynam., 44, 1789–1800, doi:10.1007/s00382-014-2312-4, 2015. 12652

Vetter, T., Huang, S., Aich, V., Yang, T., Wang, X., Krysanova, V., and Hattermann, F.: Multi-model climate impact assessment and intercomparison for three large-scale river basins on three continents, Earth Syst. Dynam., 6, 17–43, doi:10.5194/esd-6-17-2015, 2015. 12652

Vidal, J.-P., Martin, E., Franchistéguy, L., Baillon, M., and Soubeyroux, J.-M.: A 50-year high-resolution atmospheric reanalysis over France with the Safran system, Int. J. Climatol., 30, 1627–1644, doi:10.1002/joc.2003, 2010. 12656

Vidal, J.-P., Martin, E., Kitova, N., Najac, J., and Soubeyroux, J.-M.: Evolution of spatio-temporal drought characteristics: validation, projections and effect of adaptation scenarios, Hydrol. Earth Syst. Sci., 16, 2935–2955, doi:10.5194/hess-16-2935-2012, 2012. 12655

von Storch, H. and Zwiers, F.: Statistical Analysis in Climate Research, Cambridge University Press, Cambridge, 1999. 12667

Warner, R. F.: Environmental flows in two highly regulated rivers: the Hawkesbury Nepean in Australia and the Durance in France, Water Environ. J., 28, 365–381, doi:10.1111/wej.12045, 2013. 12654

Whitfield, P. H.: Is 'Centre of Volume' a robust indicator of changes in snowmelt timing?, Hydrol. Process., 27, 2691–2698, doi:10.1002/hyp.9817, 2013. 12668

Wickham, H.: ggplot2: Elegant Graphics for Data Analysis, Use R!, Springer, New York, doi:10.1007/978-0-387-98141-3, 2009. 12675

Wickham, H.: ggplot2, WIREs Comput. Stat., 3, 180–185, doi:10.1002/wics.147, 2011. 12675

Wickham, H.: Tidy data, J. Stat. Softw., 59, 1–23, 2014a. 12675

Wickham, H.: tidyr: Easily Tidy Data with spread() and gather() Functions., R package version 0.2.0, 2014b. 12675

Wickham, H. and François, R.: dplyr: A Grammar of Data Manipulation, R package version 0.4.1, 2015. 12675

Wilby, R. L. and Dessai, S.: Robust adaptation to climate change, Weather, 65, 180–185, doi:10.1002/wea.543, 2010. 12651

Wilby, R. L. and Harris, I.: A framework for assessing uncertainties in climate change impacts: low-flow scenarios for the River Thames, UK, Water Resour. Res., 42, W02419, doi:10.1029/2005WR004065, 2006. 12652

HESSD
12, 12649–12701, 2015

WMO: Manual on low-flow estimation and prediction, Operational Hydrology Report 30, WMO-No 1029, WMO, Geneva, Switzerland, 2008. 12657

Yip, S., Ferro, C. A. T., and Stephenson, D. B.: A simple, coherent framework for partitioning uncertainty in climate predictions, J. Climate, 24, 4634–4643, doi:10.1175/2011JCLI4085.1, 2011. 12652

HESSD

12, 12649–12701, 2015

Table 1. Global model runs under the A1B emissions scenario.

Acronym	Institute	GCM name	Number of runs	Reference
CNCM33	CNRM (France)	CNRM-CM3.3	1	Salas-Mélia et al. (2005)
EGMAM2	FUB (Germany)	EGMAM+	1	Huebener et al. (2007)
IPCM4	IPSL (France)	IPSL-CM4_v2	3	Marti et al. (2010)
ECHAM5	DMI (Denmark) & MPI (Germany)	ECHAM5-C	6	Roeckner et al. (2006)

HESSD
12, 12649–12701, 2015

Table 2. Statistical downscaling methods.

Acronym	Institute	Method name	Description	Reference
analog	EDF/LTHE	analog20	Analogues	Obled et al. (2002)
dsclim	CERFACS	dsclim11a2	Weather types + transfer functions	Boé et al. (2006)
d2gen	LTHE	d2gen22	Transfer functions + analogues	Mezghani and Hingray (2009)

HESSD
12, 12649–12701, 2015

Table 3. Hydrological model characteristics.

Acronym	Project partner	Type	Distributed	Snow component	Reference
GR5J	Irstea HBAN	Conceptual	No	Degree-day	Pushpalatha et al. (2011)
MORDOR	EDF DTG	Conceptual	No	Degree-day	Garçon (1999)
CEQUEAU	EDF R&D	Conceptual	Yes	Degree-day	Hendrickx (2001)
J2000	Irstea HHLY	Conceptual	Yes	Degree-day	Krause (2002)
CLSM	UMR METIS	Physically-based	Yes	Energy balance[a]	Ducharne et al. (2000)
ORCHIDEE	UMR METIS	Physically-based	Yes	Energy balance[b]	Krinner et al. (2005)

[a] 3-layer physically-based snow model.
[b] 1-layer snow model with constant properties.

HESSD
12, 12649–12701, 2015

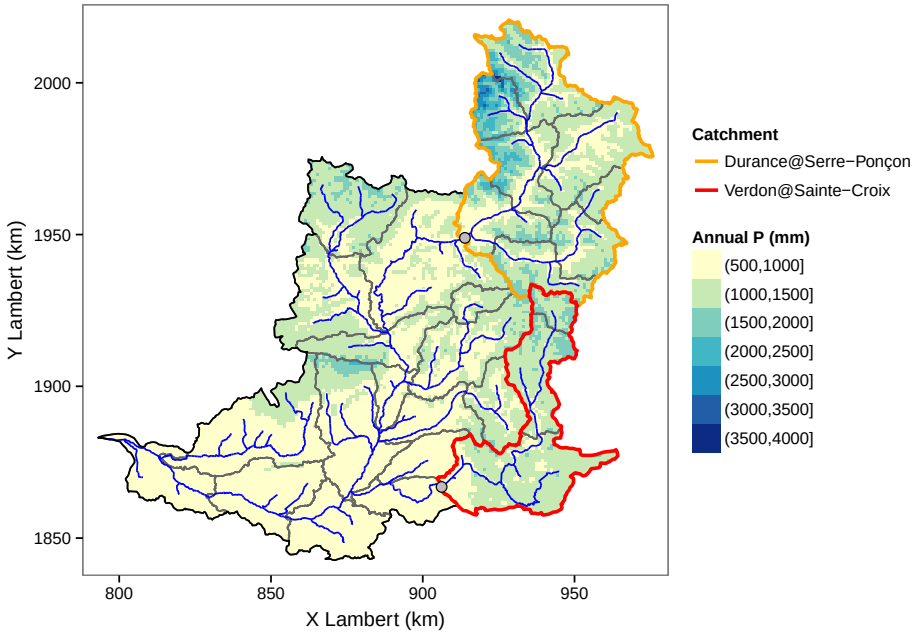

Figure 1. Delineation of the Durance basin and the two case study catchments drawn on the gridded map of the 1980–2009 mean annual precipitation from the SPAZM reanalysis (Gottardi et al., 2012).

HESSD
12, 12649–12701, 2015

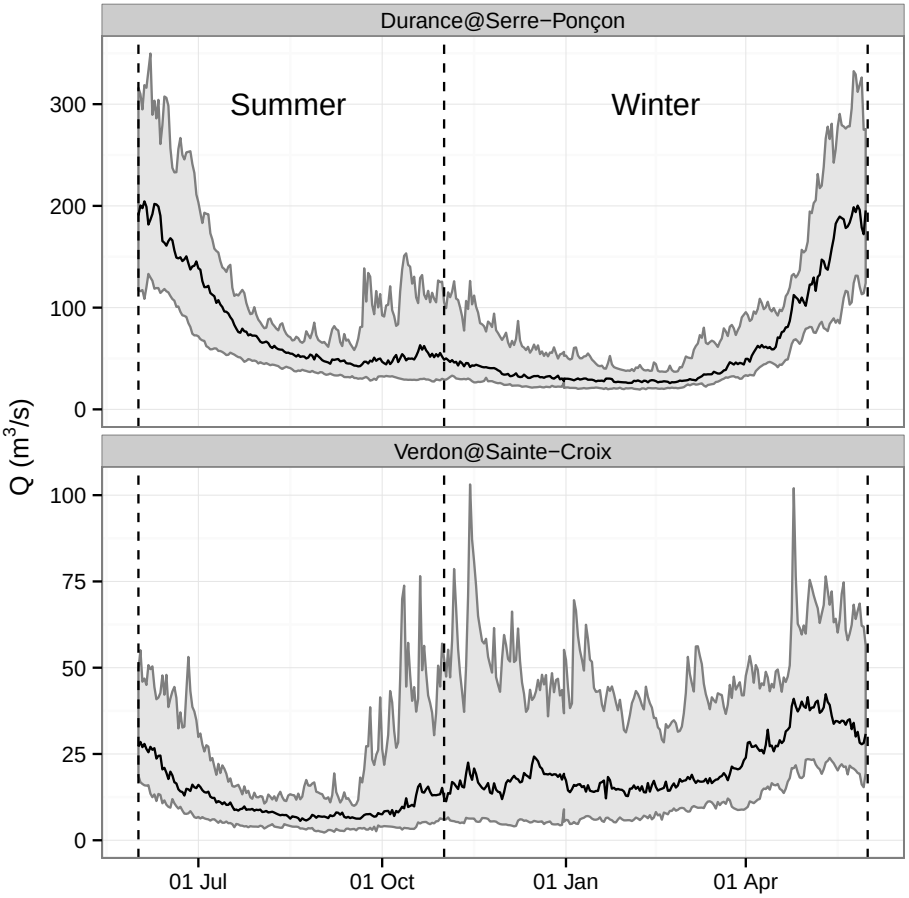

Figure 2. Daily interannual regime over the REF period for the two catchment case studies and season boundaries for low flow analysis. Grey ribbons frame the first and last deciles and the black line shows the median value.

HESSD
12, 12649–12701, 2015

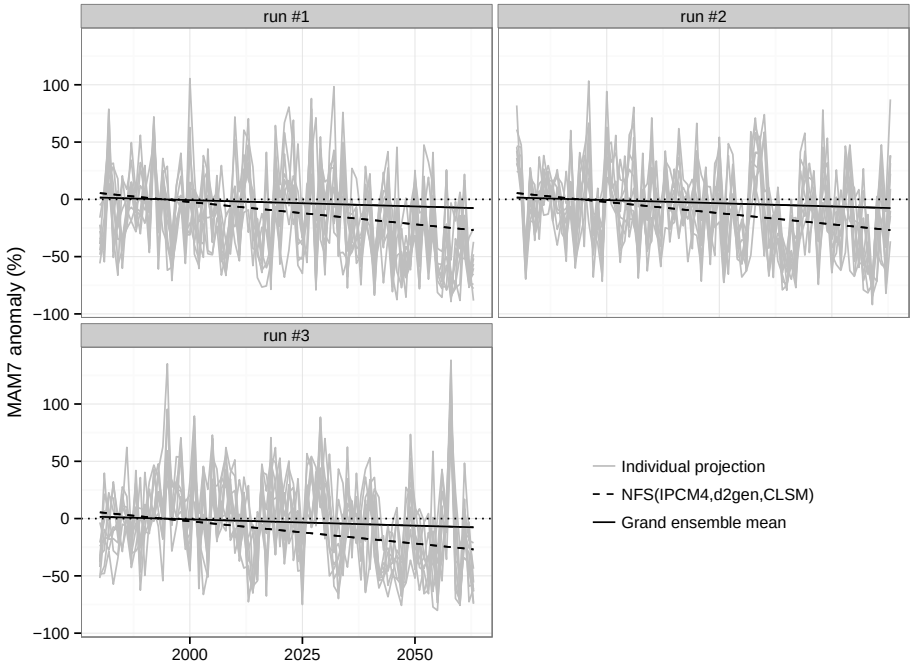

Figure 3. Winter low flow NFS(g = IPCM4, s = d2gen, h = CLSM) for the Durance@Serre-Ponçon, fitted to all 30 projections available as combinations of the IPCM4 GCM (3 runs), the d2gen SDM (10 realizations) and the CLSM hydrological model. Each panel shows 10 d2gen realizations from a given IPCM4 run as well as the common NFS and the grand ensemble mean.

HESSD
12, 12649–12701, 2015

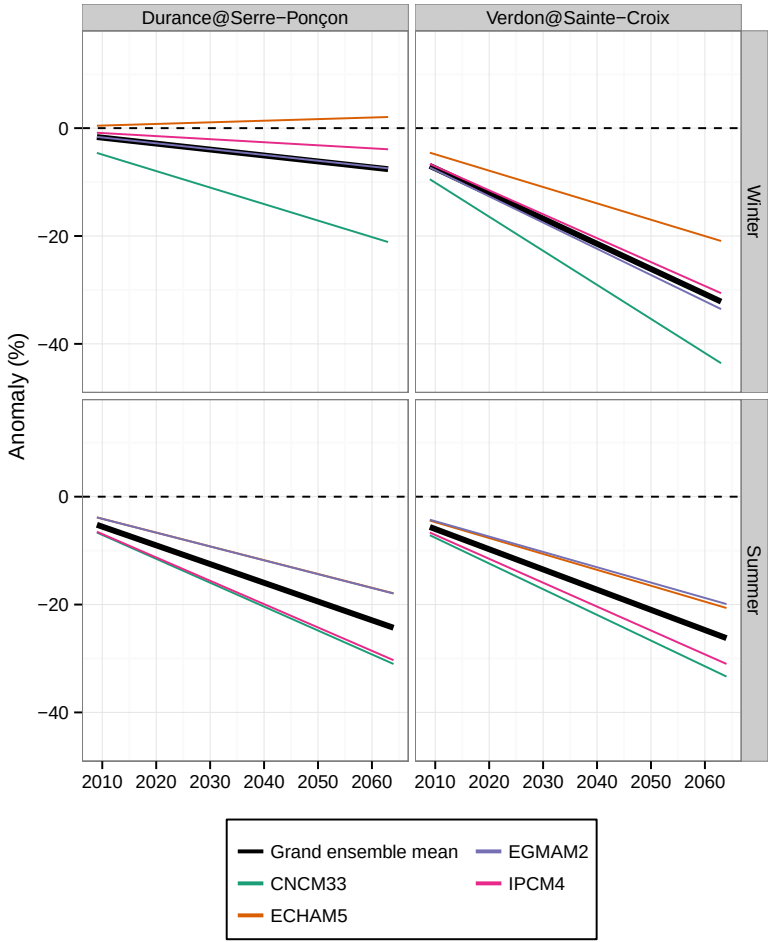

Figure 4. GCM effects on low flow changes around the grand ensemble mean for both cacthments and both seasons.

HESSD
12, 12649–12701, 2015

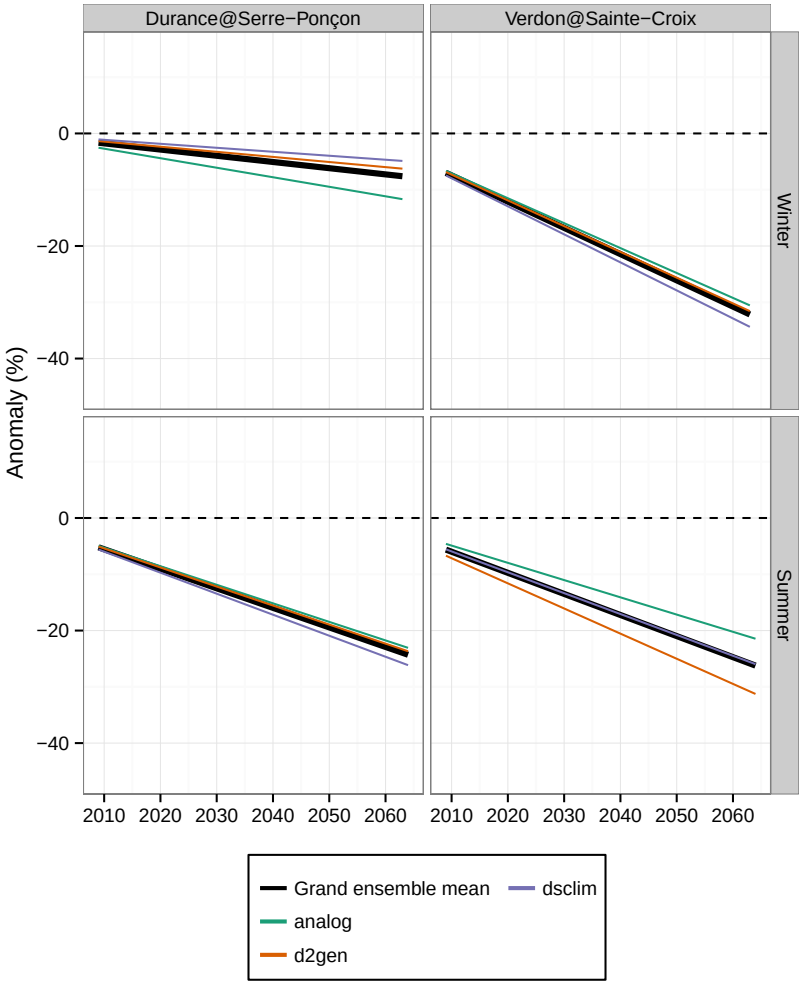

Figure 5. As for Fig. 4, but for SDM effects.

HESSD
12, 12649–12701, 2015

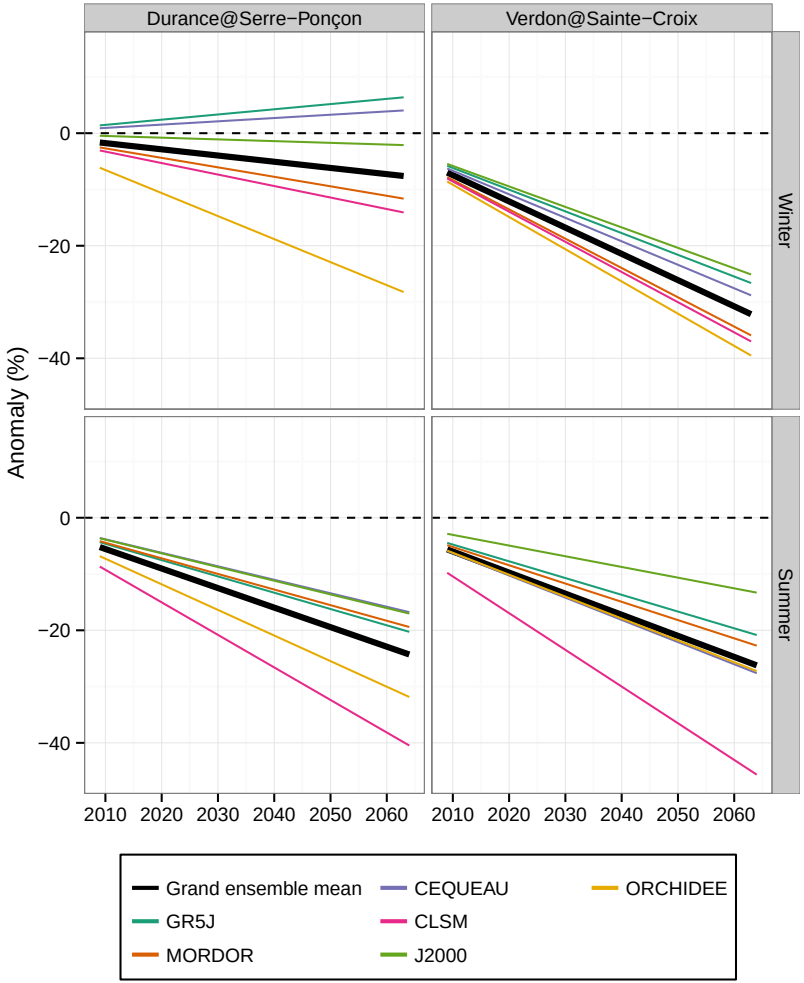

Figure 6. As for Fig. 4, but for HM effects.

HESSD
12, 12649–12701, 2015

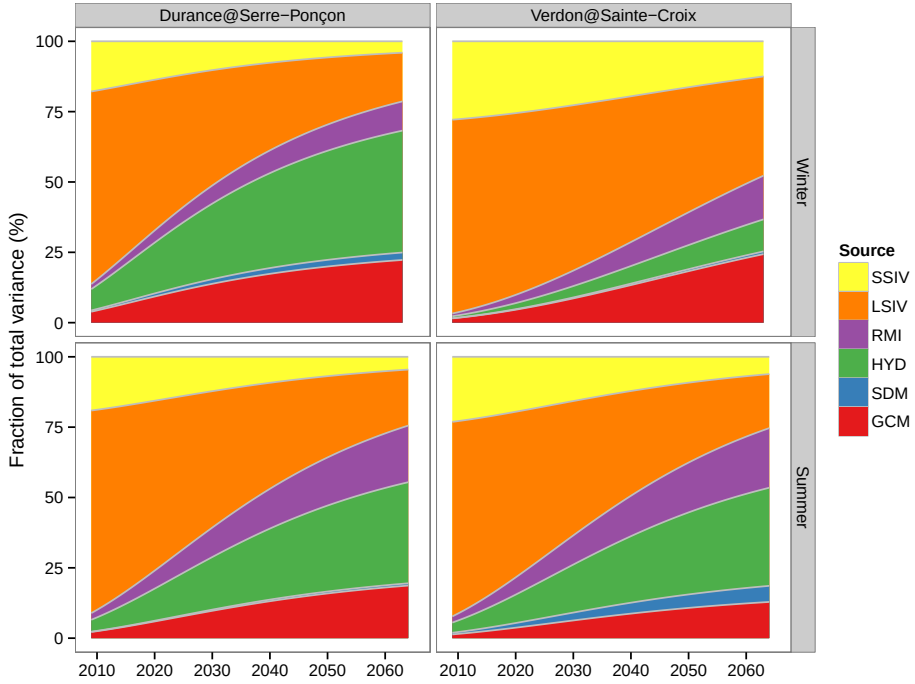

Figure 7. Fraction of total variance explained by each source of uncertainty for rolling 30 year time-slice averages of low flow changes with respect to the REF period average. Values are plotted in the middle of each time slice.

HESSD
12, 12649–12701, 2015

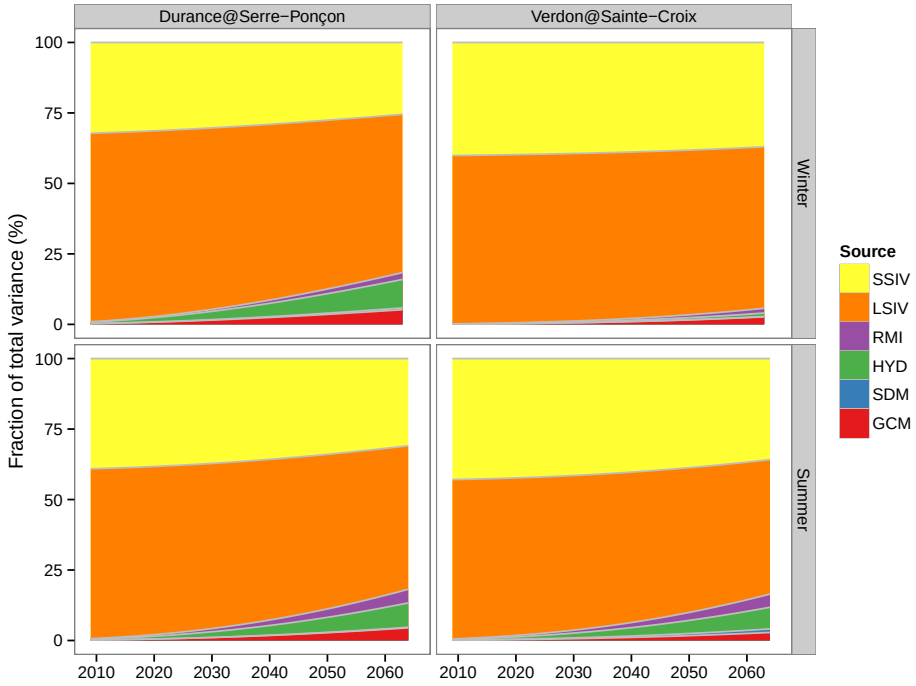

Figure 8. As for Fig. 7, but for yearly low flow anomaly with respect to the REF period average.

HESSD
12, 12649–12701, 2015

Hierarchy of climate and hydrological uncertainties in transient low flow projections

J.-P. Vidal et al.

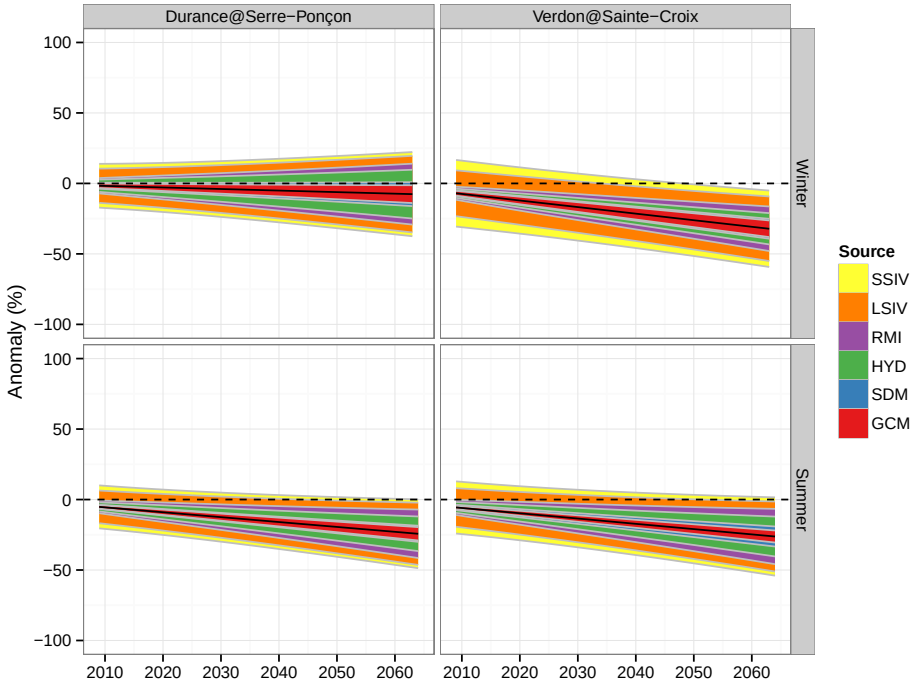

Figure 9. Projected changes in 30 year averages of low flow for both stations and seasons, together with a partitioning of the 90 % confidence interval into the different uncertainty sources. See text for details. Values are plotted in the middle of each time slice. The fraction of the confidence interval for a given source of uncertainty is proportional to the standard deviation of its contribution to the total standard deviation, following Hawkins and Sutton (2011) and Hingray and Saïd (2014).

HESSD
12, 12649–12701, 2015

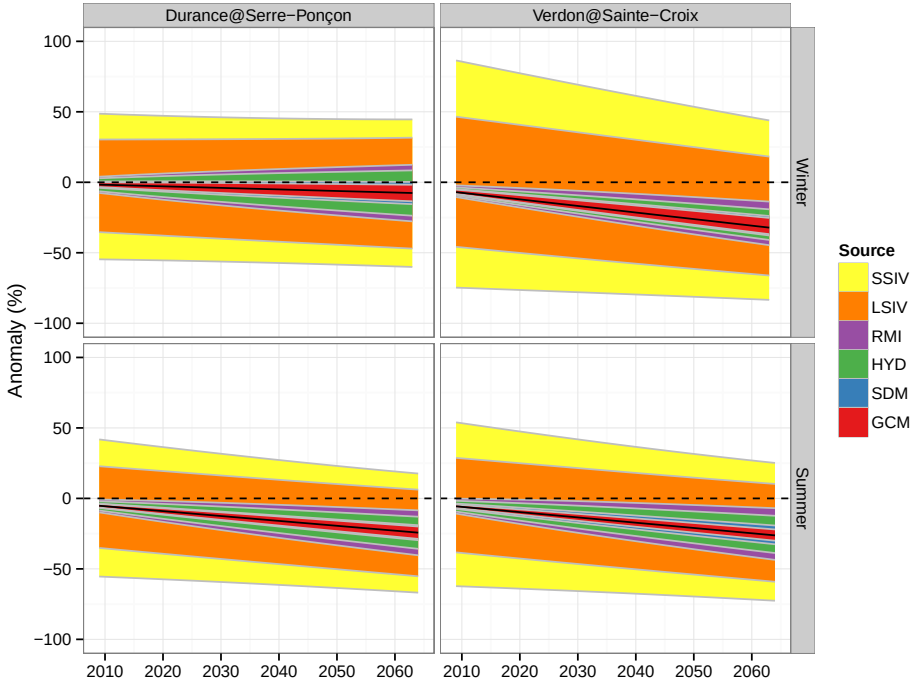

Figure 10. As for Fig. 9, but for yearly anomalies.

HESSD
12, 12649–12701, 2015

Hierarchy of climate and hydrological uncertainties in transient low flow projections

J.-P. Vidal et al.

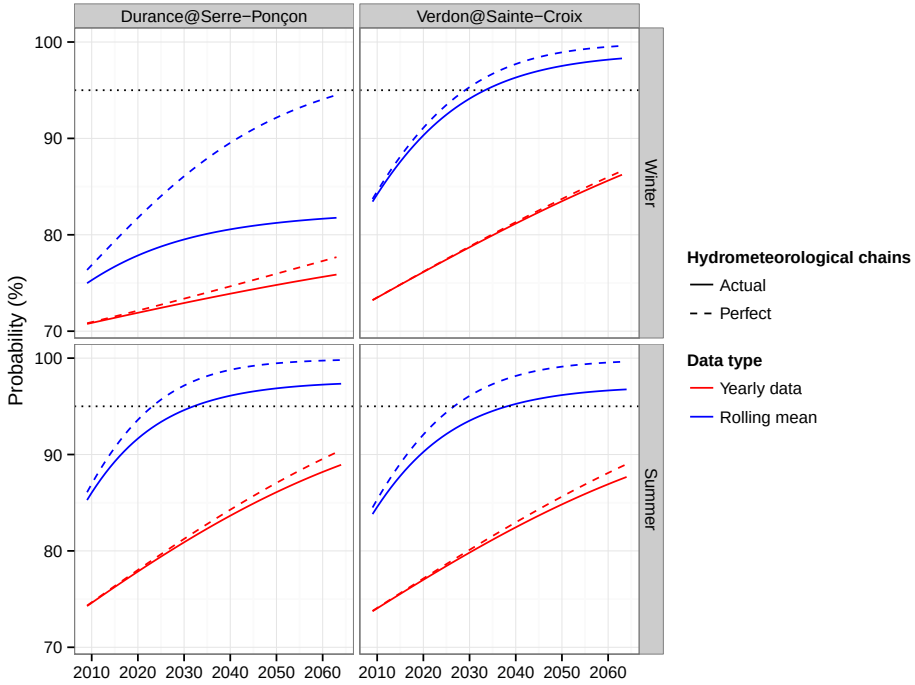

Figure 11. Evolution of the probability of a low flow below the REF period average, for yearly anomalies and 30 year rolling time-slice averages, with the hydrometeorological model chains used here and with a perfect hydrometeorological model. See text for details.

HESSD
12, 12649–12701, 2015

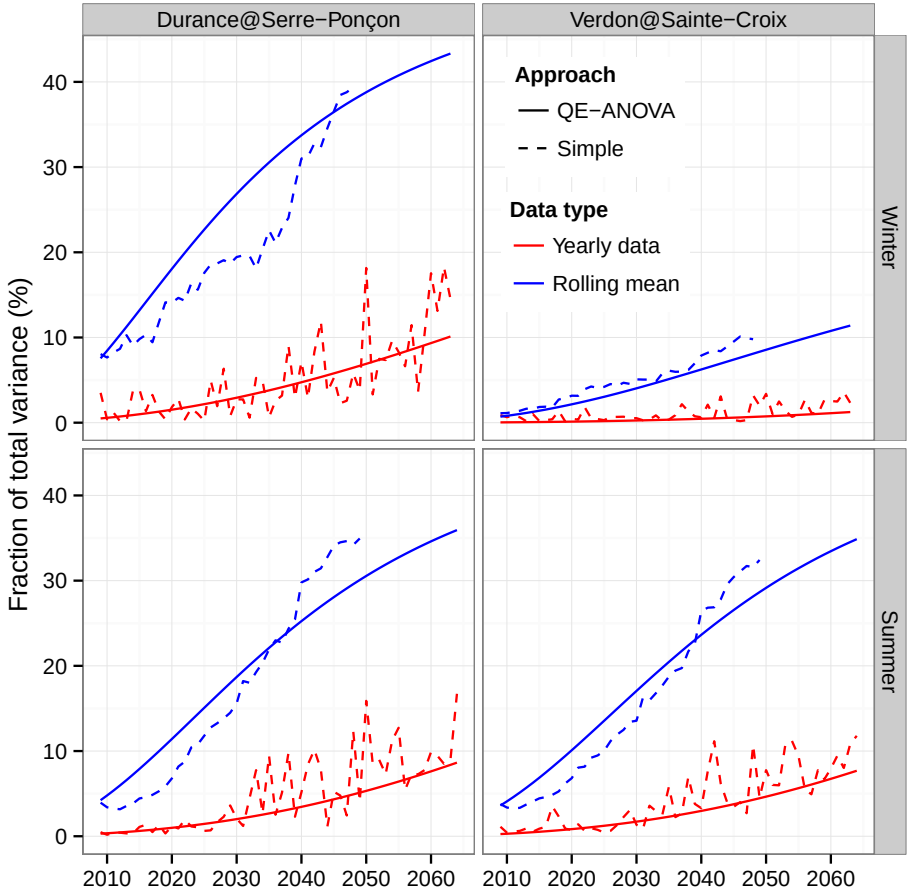

Figure 12. Fraction of total uncertainty due to hydrological models computed from the QE-ANOVA and a simpler approach (see text for details), for both yearly anomalies and changes in 30 year rolling averages.

HESSD
12, 12649–12701, 2015

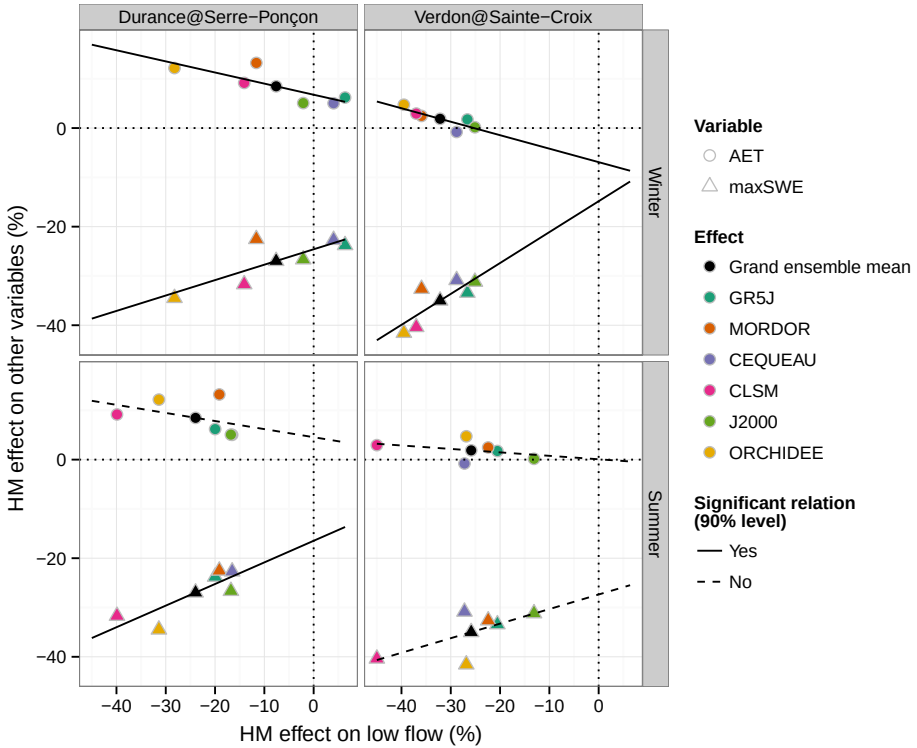

Figure 13. Relations between HM effects on low flow anomaly and HM effects on AET/maxSWE anomaly for year 2065. Significant relations at the 90 % confidence level are shown with solid lines.

HESSD
12, 12649–12701, 2015